

Measurement report: Three-year characteristics of sulfuric acid in urban Beijing and derivation of daytime sulfuric acid proxies applicable to inland sites

Yishuo Guo^{1,2}, Chao Yan^{2,3*}, Chang Li², Chenjuan Deng⁴, Ying Zhang^{2,3}, Ying Zhou², Haotian Zheng⁴, Yueqi Jiang⁴, Xin Chen², Wei Ma², Nina Sarnela⁵, Zhuohui Lin², Chenjie Hua², Xiaolong Fan⁶, Feixue Zheng², Zemin Feng², Zongcheng Wang², Yusheng Zhang², Jingkun Jiang⁴, Bin Zhao⁴, Markku Kulmala^{2,3,5}, Yongchun Liu^{2*}

Affiliations:

¹ College of Environmental and Chemical Engineering, Hebei Vocational University of Industry and Technology, Shijiazhuang, Hebei, China

² Aerosol and Haze Laboratory, Beijing Advanced Innovation Center for Soft Matter Science and Engineering, Beijing University of Chemical Technology, Beijing, China

³ Nanjing-Helsinki Institute in Atmospheric and Earth System Sciences, Nanjing University, Suzhou, China.

⁴ State Key Joint Laboratory of Environment Simulation and Pollution Control, State Environmental Protection Key Laboratory of Sources and Control of Air Pollution Complex, School of Environment, Tsinghua University, Beijing 100084, China

⁵ Institute for Atmospheric and Earth System Research / Physics, Faculty of Science, University of Helsinki, Finland

⁶ Center for Excellence in Regional Atmospheric Environment, Key Lab of Urban Environment and Health, Institute of Urban Environment, Chinese Academy of Sciences, Xiamen, China

*Correspondence to: Chao Yan (chaoyan@nju.edu.cn), Yongchun Liu (liuyc@buct.edu.cn)

Abstract Sulfuric acid (H_2SO_4) is a key precursor in atmospheric new particle formation and cluster early growth. However, long-term measurement of it is only available at a few sites. Although several proxies for estimating H_2SO_4 concentration have been proposed, they are always site-specific. Therefore, both reliable H_2SO_4 measurement and proxies with wider application are highly needed. Here, we conducted a long-term H_2SO_4 measurement in urban Beijing during 2019–2021, and derived three H_2SO_4 proxies based entirely on its formation and loss pathways. Results show that daytime H_2SO_4 concentration is $2.0\text{--}7.4 \times 10^6$ molec cm^{-3} and shows an overall decline with an average annual decrease of 14%. This decline is mainly due to the ongoing SO_2 emission controls. Daytime H_2SO_4 shows a clear seasonal variation that tracks UVB. Nighttime H_2SO_4 concentration is $1.6\text{--}6.3 \times 10^5$ molec cm^{-3} , with higher levels in warmer seasons due to stronger sources and lower condensation sink (CS). The diurnal variations of H_2SO_4 across seasons follow those of photo-oxidation-related parameters, such as UVB, OH radical, and photolysis rate of NO_2 ($J(\text{NO}_2)$). All of the three proxies can reproduce H_2SO_4 concentration during 10:00–14:00. Importantly, they can estimate H_2SO_4 concentration at a boreal forest site in Hyytiälä, Finland, suggesting their applicability to sites with diverse environments. Furthermore, the parameters used in UVB- $\text{PM}_{2.5}$ based proxy are available at most observational sites. Further application of this proxy could provide H_2SO_4 concentrations covering many regions worldwide, which may further facilitate research on atmospheric nucleation and secondary aerosol growth of these sites.

1. Introduction

38 New particle formation (NPF) is a key contributor to the born of atmospheric aerosols (Merikanto et al.,
39 2009;Gordon et al., 2017), and thus can have a great influence on global climate and human health (Stocker,
40 2014;Lelieveld et al., 2015). Among all the precursors that drive atmospheric nucleation, the initial step of NPF,
41 sulfuric acid (H_2SO_4) has been shown to be the most important one from both laboratory experiments and field
42 observations (Kulmala et al., 2006;Riipinen et al., 2007;Paasonen et al., 2009;Erupe et al., 2010;Wang et al.,
43 2011;Kirkby et al., 2011;Yu et al., 2012;Almeida et al., 2013;Kürten et al., 2014;Riccobono et al., 2014;Lehtipalo
44 et al., 2018;Yao et al., 2018;Lee et al., 2019;Myllys et al., 2019;Yan et al., 2021). The clusters formed by sulfuric
45 acid and base molecules, such as ammonia and amines, provide the primary core for further condensation of other
46 low-volatility species, promoting aerosols growth to tens of nanometers, reaching the sizes of cloud condensation
47 nuclei (CNN) and ultrafine particles. Therefore, reliable measurement of sulfuric acid is of great importance.

48 Since the 1990s, sulfuric acid measurements have been conducted in various field campaigns that covered a
49 wide range of atmospheric environments, including urban (McMurry et al., 2005;Fiedler et al., 2005;Riipinen et al.,
50 2007;Mikkonen et al., 2011;Wang et al., 2011;Yao et al., 2018;Lu et al., 2019), rural (Berresheim et al.,
51 2000;Birmili et al., 2003;Paasonen et al., 2009;Erupe et al., 2010;Mikkonen et al., 2011;Kürten et al., 2016;Yang
52 et al., 2021a;Yang et al., 2023), mountainous (Weber et al., 1996;Weber et al., 1997;Boy et al., 2008;Mikkonen et
53 al., 2011), marine (Berresheim et al., 1993;Weber et al., 1995;Weber et al., 1996;Berresheim et al., 2002;O'Dowd
54 et al., 2002), forest environments (Fiedler et al., 2005;Riipinen et al., 2007;Petäjä et al., 2009;Nieminen et al.,
55 2009;Mikkonen et al., 2011;Jokinen et al., 2012), among others (Weber et al., 1998;Mauldin et al., 2001;Mauldin
56 et al., 2004;Sarnela et al., 2015;Jokinen et al., 2018). The locations of these sites, measurement periods, and
57 corresponding sulfuric acid concentrations are summarized in Table 1. In general, within the planetary boundary
58 layer, sulfuric acid concentration was around $0.2 - 15 \times 10^6 \text{ cm}^{-3}$, with the highest levels in urban areas, followed
59 by rural, mountainous, and marine regions, and the lowest in forest areas. This suggests that sulfuric acid levels
60 depend strongly on the intensity of human activity. In addition, most measurement campaigns lasted for less than
61 four months and concentrated mostly on warmer seasons (spring, summer and early autumn) when NPF usually
62 occurs (Dal Maso et al., 2005;Manninen et al., 2009;Dada et al., 2017;Nieminen et al., 2018;Chu et al., 2019;Qi et
63 al., 2015). Previous studies showed that NPF in Chinese megacities was also frequently observed in winter (Deng
64 et al., 2020;Chu et al., 2019), and thus sulfuric acid measurement in cold seasons is also crucial. To date, however,
65 long-term measurement of sulfuric acid worldwide is still lacking, which somewhat limits the investigation of NPF
66 processes.

67 To complement the limited sulfuric acid measurement, several sulfuric acid proxies were developed. The original
68 expression for estimating sulfuric acid concentration was derived from its production and loss pathways. Assuming
69 that sulfuric acid originates solely from OH-initiated oxidation of SO_2 and the only loss is the condensation sink
70 (CS) onto particle surfaces, the steady-state concentration of sulfuric acid can be expressed as $[\text{H}_2\text{SO}_4] =$
71 $k \cdot [\text{OH}][\text{SO}_2]/\text{CS}$, where k is the rate constant of $\text{OH} + \text{SO}_2$ reaction. As early as 1997, Weber et al. estimated sulfuric
72 acid concentrations at a marine site and a mountain site using this expression (Weber et al., 1996). Results showed

73 that the estimated daytime sulfuric acid for two selected days generally matched the measured one at both sites.
 74 Later, Berresheim et al. also utilized this expression at a coastal site (Berresheim et al., 2002). However, when the
 75 accommodation coefficient of CS calculation was chosen as 1, the estimated sulfuric acid concentration turned out

76 **Table 1.** Summary of atmospheric sites with sulfuric acid measurement.

Type of Site	Location	Measurement Period	H ₂ SO ₄ (× 10 ⁶ molec cm ⁻³)	References
Urban	Atlanta, Georgia, USA	2002/08	2.9	2005, McMurry et al. 2011, Mikkonen et al.
	Heidelberg, Germany	2004/03 - 04	3.0	2005, Fiedler, et al. 2007, Riipinen et al.
	Beijing, China	2008/07 - 09	1.0 - 9.0	2011, Wang et al.
	Shanghai, China	2014/03 - 2016/02	7.8	2018, Yao et al.
	Beijing, China	2018/02 - 03	4.9	2019, Lu, et al.
Rural	Hohenpeissenberg, Germany	151 days in 1998 186 days in 1999	0.1 -10	2000, Berresheim et al.
		1998/04 - 2000/07	0.6	2003, Birmili et al. 2009, Paasonen et al. 2011, Mikkonen et al.
	Ohio, USA	2008/08 - 2009/11	winter: 0.6 spring: 5.2 summer: 2.9 autumn: 0.5	2010, Erupe et al.
	San Pietro Capofiume, Italy	2009/06 - 07	2.4	2011, Mikkonen et al.
	Melpitz, Germany	2008/05	2.9	2011, Mikkonen et al.
	Vielbrunn, Germany	2014/05 - 06	3.0	2016, Kürten et al.
	Nanjing, China	2017/12 - 2018/01	winter: 1.9 spring: 7.4 summer: 4.5 autumn: 9.0	2021, Yang et al.
		2018/04		
		2018/07 - 08		
	Xiamen, China	2022/07 - 08	2.3	2023, Yang et al.
Mountain	Colorado, USA	1993/09	0.1 - 10	1996, Weber et al. 1997, Weber et al.
		2006/06 - 07	2.8	2008, Boy et al.
		2007/06 - 07	1.4	2011, Mikkonen et al.
Marine	Washington, USA	1991/04	0.03 - 32.0	1993, Berresheim et al.
	Hawaii, USA	1992/07	upslope: 1.2 downslope: 0.5	1995, Weber et al. 1996, Weber et al.
		1999/06	1.5	2002, Berresheim et al.
	Mace Head, Ireland	1998/09 1999/06	2.0 - 15.0	2002, O'Wowd et al.
Forest	Hyytiälä, Finland	2003/03 - 04	2.6	2005, Fiedler et al.
		2005/04 - 05	1.0 - 10	2007, Riipinen et al.
		2007/03 - 06	0.9 - 2.5	2009, Petäjä et al. 2009, Nieminen et al.
		2003/03 - 04	0.6	2011, Mikkonen et al.
		2007/03 - 06	0.2	2011, Mikkonen et al.
		2011/03 - 04	0.3 - 10	2012, Jokinen et al.
Others	Macquarie Island, Australia	11/27/1995	2.8	1998, Weber et al.
	Antarctica	1998/12	0.3	2001, Mauldin III et al.
		2000/11 - 12	0.3	2004, Mauldin III et al.
		2014/11 - 2015/01	0.2 - 10	2018, Jokinen et al.
	Kilpilahti, Finland	2012/06 - 07	oil refinery: 11.5 industrial: 4.4 non-industrial: 1.3	2015, Sarnela et al.

77 to be much lower than the measured one. The authors speculated that additional sulfuric acid sources might exist,
 78 likely the OH- or BrO-initiated oxidation of dimethyl disulfide or dimethyl sulfide, or the oxidation of SO₂ by non-
 79 OH oxidants. This also suggests that this proxy may not be suitable for coastal environments. In 2009, Petäjä et al.
 80 proposed the concept of sulfuric acid proxy clearly and derived three proxies based on its source-sink equilibrium
 81 (Petäjä et al., 2009). The first proxy, $P_1 = k_1 \cdot [\text{OH}][\text{SO}_2]/\text{CS}$, was very similar to that proposed by Weber et al., but
 82 the pre-factor k_1 was obtained by the fitting of measurement data. During daytime, OH radical mainly arises from
 83 photochemical reactions. Therefore, OH radical in P_1 could be replaced by UVB, yielding the second proxy of $P_2 =$
 84 $k_2 \cdot [\text{UVB}][\text{SO}_2]/\text{CS}$. Similarly, replacing OH radical with global radiation yielded the third proxy, $P_3 =$
 85 $k_3 \cdot [\text{Glob}][\text{SO}_2]/\text{CS}$. These three proxies showed good performance in estimating daytime sulfuric acid concentration.
 86 However, the authors noted that k_1 , k_2 and k_3 came from fits so that they are likely site-specific, which limits their
 87 transferability to other sites.

88 Later, Mikkonen et al. attempted to develop sulfuric acid proxies suitable for various environments. The datasets
 89 came from five sites, including one forest, one mountainous, two rural and one urban sites (Mikkonen et al., 2011).
 90 Five linear-fitting proxies, including one (Eq. 1) similar to the P_3 proxy proposed by Petäjä et al., were first built.

$$91 \quad L1 = B \cdot k \cdot \text{Radiation} \cdot [\text{SO}_2] \cdot \text{CS}^{-1} \quad (1)$$

92 Results showed only minor differences among the five proxies, with L3 proxy (Eq. 2) generally performing the best.

$$93 \quad L3 = B \cdot k \cdot \text{Radiation} \cdot [\text{SO}_2]^{0.5} \quad (2)$$

94 Based on this, the authors concluded that the pseudo-steady-state assumption for gaseous sulfuric acid could be
 95 somewhat unrealistic in atmospheric conditions, and then proposed five additional nonlinear-fitting sulfuric acid
 96 proxies. However, only correlation coefficients were used to evaluate the performance of five linear fitting proxies,
 97 and these correlation coefficients were close to each other. Thus, the above conclusion requires more data to be
 98 supported.

99 Based on these studies, Lu et al. developed seven nonlinear-fitting proxies to estimate daytime sulfuric acid
 100 concentration in urban Beijing (Lu et al., 2019). In proxies of N5–N7, O₃ and HONO were included to account for
 101 OH radical formation via photolysis of HONO. Results showed that seven proxies generally performed well in
 102 estimating daytime sulfuric acid concentration with similar correlation coefficients and relative errors. Nevertheless,
 103 the authors concluded that N7 proxy (Eq. 3) was the most suitable for estimating daytime sulfuric acid, as it took
 104 the CS loss pathway into account, had the lowest relative error and used the easily measured NO_x.

$$105 \quad [\text{H}_2\text{SO}_4] = 0.0013 \cdot \text{UVB}^{0.13} \cdot [\text{SO}_2]^{0.40} \cdot \text{CS}^{-0.17} \cdot ([\text{O}_3]^{0.44} + [\text{NO}_x]^{0.41}) \quad (3)$$

106 Note that this proxy was developed for urban Beijing, and thus may not apply to other sites. A year later, Dada et al.
 107 constructed proxies based on the source-sink equilibrium of sulfuric acid at four different sites, including one
 108 boreal forest, one rural, one urban, and one megacity sites. The formation of sulfuric acid from the ozonolysis of
 109 alkenes was first considered. Results showed that P_1 (Eq. 4) and P_3 (Eq. 5) proxies with the alkene ozonolysis term
 110 could estimate both daytime and nighttime sulfuric acid well, while P_2 proxy (Eq. 6) without the alkene ozonolysis
 111 term could only estimate daytime sulfuric acid.

$$112 \quad ([\text{H}_2\text{SO}_4] = -\frac{\text{CS}}{2k_3} + \sqrt{\left(\frac{\text{CS}}{2k_3}\right)^2 + \frac{[\text{SO}_2]}{k_3} (k_1 \cdot \text{GlobRad} + k_2 \cdot [\text{O}_3][\text{Alkenes}]}) \quad (4)$$

$$113 \quad [\text{H}_2\text{SO}_4] = \frac{k_1 \cdot \text{GlobRad}[\text{SO}_2] + k_2 \cdot [\text{SO}_2][\text{O}_3][\text{Alkene}]}{\text{CS}} \quad (5)$$

$$114 \quad [\text{H}_2\text{SO}_4] = -\frac{\text{CS}}{2k_3} + \sqrt{\left(\frac{\text{CS}}{2k_3}\right)^2 + \frac{[\text{SO}_2]}{k_3} k_1 \cdot \text{GlobRad}} \quad (6)$$

115 Although the proxy equations were the same across sites, the parameters therein were different. Thus, these four
116 proxies have limited application at other sites.

117 In this study, we characterize the interannual, seasonal, and diurnal variations of sulfuric acid in urban Beijing
118 and derive proxies to estimate sulfuric acid concentration at various sites. Long-term measurement of sulfuric acid
119 covering nearly three continuous years (from 1st January, 2019 to 11th November, 2021) was conducted in urban
120 Beijing. First, the yearly and seasonal variation of sulfuric acid concentration, as well as its diurnal cycles were
121 analyzed. Second, the performance of nine representative proxies, including seven steady-state based ones and two
122 numerical regression ones, from previous studies at our site was investigated. Based on these analyses, three steady-
123 state proxies were proposed according to the budget analysis of sulfuric acid, and their performance and limitations
124 on estimating daytime sulfuric acid concentration were investigated in detail. These three proxies were then applied
125 to estimate sulfuric acid concentration at a boreal forest site in Hyytiälä, Finland. Correlation coefficients and
126 relative errors indicate that three proxies are able to reproduce daytime sulfuric acid well, suggesting that three
127 proxies and parameters therein could be applicable at other atmospheric sites. Finally, a general suggestion on proxy
128 selection with different available parameters was given.

129 2. Method

130 2.1 Measurement site

131 The measurements were conducted at the Aerosol and Haze Laboratory at the west campus of Beijing University
132 of Chemical Technology (39.95° N, 116.31° E). It is a typical urban site surrounded by commercial and residential
133 areas and three major roads (Liu et al., 2020; Yan et al., 2021; Guo et al., 2021; Yan et al., 2022). The datasets used
134 in this study span nearly three continuous years from January 2019 to November 2022.

135 2.2 Measurement of sulfuric acid

136 Sulfuric acid was measured by a long time-of-flight chemical ionization mass specter (LTOF-CIMS, Aerodyne
137 Research, Inc.) using nitric acid as reagent ions. The basic working principle of this instrument is described
138 elsewhere (Jokinen et al., 2012), and the instrument configuration has been provided in our previous studies and
139 has remained unchanged over the years. Briefly, air was drawn through a stainless-steel tube (1.6 m long, 3/4 inch
140 in diameter). The inlet flow rate was maintained at 7.2 L min⁻¹. Additionally, a flush plate (Karsa Inc.) was installed
141 to effectively remove water vapor in the sampled air.

142 Sulfuric acid concentration was quantified from the ratio of bisulfate ions (with counting rates unit in ions s⁻¹)
143 to primary ions as follows:

$$\text{H}_2\text{SO}_4 = \frac{\text{HSO}_4^- + \text{H}_2\text{SO}_4\text{NO}_3^-}{\text{NO}_3^- + \text{HNO}_3\text{NO}_3^- + (\text{HNO}_3)_2\text{NO}_3^-} \times C \quad (7)$$

144
 145 where C is the calibration coefficient, determined by direct calibration using known amounts of gaseous sulfuric
 146 acid injected into the instrument (Kürten et al., 2012). During the measurement period, the instrument ran stably.
 147 Calibration was performed every six months and after tuning. After correcting the diffusional wall loss of the
 148 sampling line (0.2129), the final calibration coefficients were $6.07 - 7.47 \times 10^9$ molec cm^{-3} over the three-year
 149 period.

150 2.3 Other ancillary measurements

151 Particle number concentration and size distribution was measured by a differential mobility particle sizer (DMPS,
 152 6 – 840 nm) (Aalto et al., 2001) and a particle size distribution system (PSD, 3 nm – 10 μm) (Liu et al., 2016). The
 153 configuration of these two instruments have been described in our previous studies (Zhou et al., 2021, Yan et al.,
 154 2021). Based on these measurements, the condensation sink (CS) of sulfuric acid can be calculated from the
 155 following Eq. (8) (Kulmala et al., 2012):

$$CS = 4\pi D \int_0^{d_p^{max}} \beta_m(d'_p) d'_p N_{d'_p} dd'_p = 4\pi D \sum_{d'_p} \beta_{m,d'_p} d'_p N_{d'_p} \quad (8)$$

156
 157 where D is the diffusion coefficient of sulfuric acid, d'_p is the particle diameter, $N_{d'_p}$ is the particle number
 158 concentration with diameter d'_p , and β_m represents the transition-regime correction. Size-resolved hygroscopic
 159 growth of aerosols was considered in the calculation of CS. CS values calculated from two instruments are shown
 160 in Figure S13. The datasets from PSD was chosen in priority as it measures wider size ranges. If PSD data was
 161 unavailable or not consecutive for more than 10–20 days, DMPS data was used. There were three periods during
 162 which measurements from both instruments were continuous and stable, and the CS comparison for these periods
 163 are shown in Figure S14. Compared with PSD CS values, DMPS CS values were on average $\sim 11.7\%$ lower.

164 Meteorological parameters were measured by a weather station (AWS310, Vaisala Inc.) located on the building
 165 rooftop. These parameters include ambient temperature, relative humidity (RH), pressure, visibility, UVB radiation,
 166 and horizontal wind speed and direction. Trace gases, including carbon monoxide (CO), sulfur dioxide (SO₂),
 167 nitrogen oxides (NO_x), and ozone (O₃), were monitored using four Thermo Environmental Instruments (models 48i,
 168 43i-TLE, 42i, 49i, respectively). Calibrations of these instruments were performed every two weeks using standard
 169 gases of known concentrations. The mass concentration of PM_{2.5} and PM₁₀ were measured with a tapered element
 170 oscillating microbalance dichotomous ambient particulate monitor (TEOM 1405-DF, Thermo Fisher Scientific Inc,
 171 USA). The mass concentration of PM_{coarse} was obtained based on the difference between PM₁₀ and PM_{2.5}.

172 2.4 Modelling of OH radical, J(NO₂) and J(O¹D)

173 The Weather Research and Forecasting Model-Community Multiscale Air Quality (WRF-CMAQ) model was
 174 applied to simulate the concentration of OH radical, the photolysis rate of NO₂ (J(NO₂)) and the photolysis rate for
 175 producing excited atomic oxygen from O₃ (J(O¹D)). Simulations covered the period from 1st January, 2019 to 19th
 176 February, 2020. The physical options in WRF (version 3.9.1) were the same as in Zheng et al. (2019a). The CMAQ

177 model (version 5.3.2) was coupled with the two-dimensional Volatility Basis Set (2D-VBS) (Zhao et al., 2016),
178 where the SAPRC07 mechanism was adopted for gas-phase chemistry, and the AERO6 (Sarwar et al., 2011) was
179 used for aerosol module. The modelling domain was the same as in Zheng et al. (2020), where the horizontal
180 resolution was $27 \text{ km} \times 27 \text{ km}$ and the vertical grid had 14 layers. Default planetary boundary layer settings were
181 used. To minimize the influence of initial conditions, simulations were spun up 5 days before the modelling period.
182 This WRF-CMAQ model and the emission inventory have been widely applied and validated in previous studies
183 using multiple lines of evidence, including ground-based monitoring networks and satellite retrievals (Zhao et al.,
184 2018;Zheng et al., 2019a, b, 2023, 2024;Chang et al., 2023). Simulated concentrations of key pollutants agree well
185 with observations in both magnitude and temporal variability (Tables S5–S7). These demonstrate that the modeling
186 system reasonably reproduces the spatial and temporal variations of major air pollutants across China.

187 **3. Results and discussion**

188 **3.1 Characteristics of measured sulfuric acid**

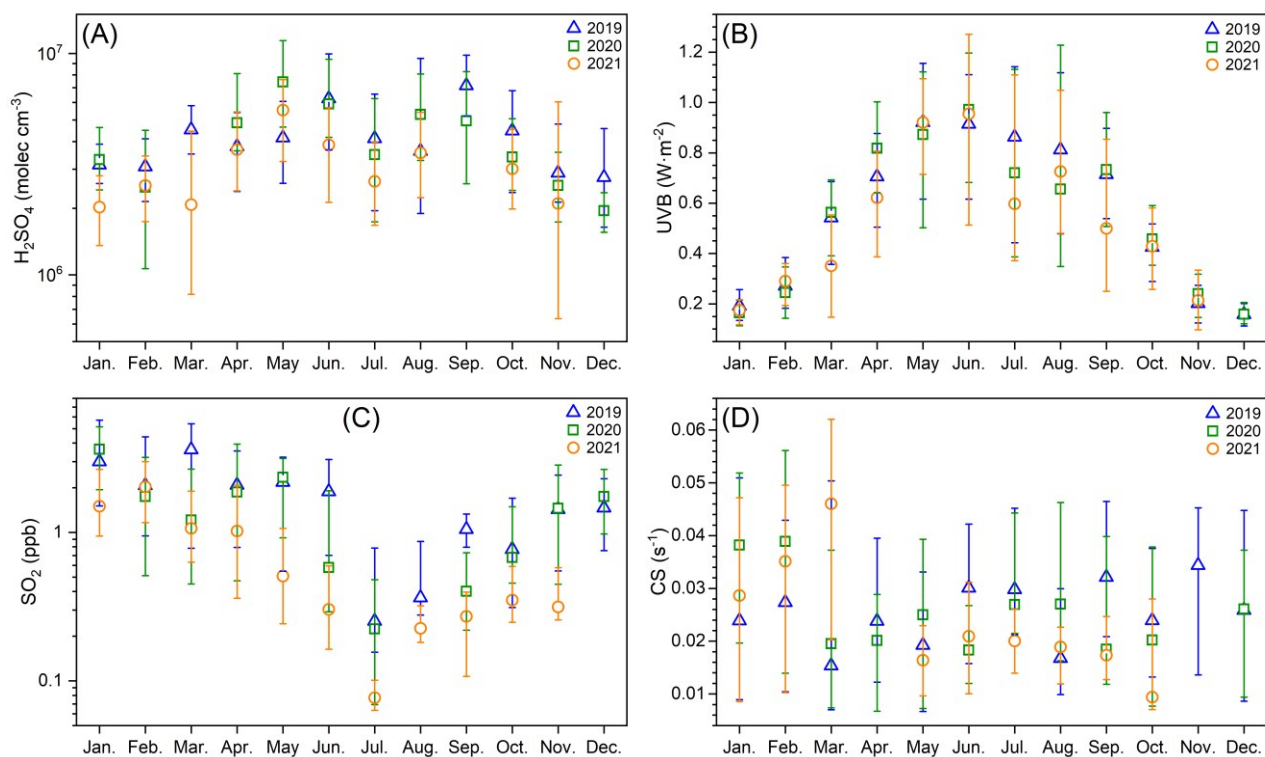
189 **3.1.1 Interannual and monthly variations of sulfuric acid**

190 In the early morning, sulfuric acid concentration is influenced not only by the photochemical production and
191 loss pathways, but also by additional sources, such as SO_2 oxidation on traffic-related black carbon (Yao et al.,
192 2020). In addition, sulfuric acid from direct emission and the ozonolysis of alkenes cannot be ignored during
193 daytime when far from noon (Yang et al., 2021a). Therefore, daytime window of 10:00–14:00 (local time) was
194 chosen for proxy evaluation unless specified otherwise. This period also corresponds to the new particle formation
195 time (Kulmala et al., 2007;Kulmala et al., 2013;Deng et al., 2020;Ma et al., 2021). The corresponding nighttime
196 window was 22:00–02:00 next day (local time).

197 In urban Beijing, typical daytime sulfuric acid concentration ranges from 2.0×10^6 to $7.4 \times 10^6 \text{ molec cm}^{-3}$
198 (monthly median concentration, Figure 1A and Table 2). Figure 1A and Figure S1E show that sulfuric acid
199 concentration generally declines from 2019 to 2021, with an average annual decrease of 14%. During the three
200 years, UVB intensity remains roughly constant (Figure 1B and Figure S1A), CS change is not significant (Figure
201 1D and Figure S1E), while SO_2 concentration decreases markedly (Figure 1C and Figure S1D). Thus, the yearly
202 decline of sulfuric acid is mainly attributed to the decrease of SO_2 (by $\sim 25\%$ per year, Table S8). Figure 1A also
203 reveals that sulfuric acid concentration has a clear seasonal variation, which is the highest in May ($4.2 - 7.4 \times 10^6$
204 molec cm^{-3}) and September ($5.0 - 7.2 \times 10^6 \text{ molec cm}^{-3}$) and the lowest from November to February of the next
205 year ($2.0 - 3.3 \times 10^6 \text{ molec cm}^{-3}$). UVB shows the same monthly pattern as sulfuric acid, which reaches the highest
206 from May to September and decreases to the lowest from November to February of next year, while SO_2 shows an
207 opposite monthly trend to sulfuric acid. This indicates that the influence of UVB on sulfuric acid monthly variation
208 outperforms that of SO_2 . Meanwhile, sulfuric acid concentration in July is much lower from May to September,
209 likely driven by extremely low SO_2 despite a small decrease of UVB in that month. In Beijing, precipitation occurs
210 more frequently in July and August than in May, June and September (Table S1). This reduces UVB and SO_2 in

211 these two months (Figure S2), and further leads to lower sulfuric acid concentration. Overall, UVB intensity and
 212 SO₂ concentration are the two key parameters determining sulfuric acid concentration.

213



214

215 **Figure 1.** Three-year (from 2019 January to 2021 November) monthly variations of (A) H₂SO₄ concentration, (B) UVB, (C)
 216 SO₂ and (D) condensation sink (CS) during daytime (10:00-14:00) when new particle formation mostly occurs. Blue triangles,
 217 green squares and orange circles represent data in 2019, 2020 and 2021, respectively. The up line, middle marker and bottom
 218 line stand for upper quartile, median and lower quartile values, respectively.

219 **Table 2.** Monthly concentration of H₂SO₄ (molec cm⁻³) during daytime (10:00-14:00) from 2019 to 2021. “NaN” means there
 220 is no data available.

Month	2019			2020			2021		
	Median	25th	75th	Median	25th	75th	Median	25th	75th
January	3.1×10 ⁶	2.6×10 ⁶	3.9×10 ⁶	3.3×10 ⁶	2.4×10 ⁶	4.6×10 ⁶	2.0×10⁶	1.4×10 ⁶	2.8×10 ⁶
February	3.1×10 ⁶	2.1×10 ⁶	4.1×10 ⁶	2.5×10 ⁶	1.1×10 ⁶	4.5×10 ⁶	2.5×10 ⁶	1.7×10 ⁶	3.4×10 ⁶
March	4.5×10 ⁶	3.5×10 ⁶	5.8×10 ⁶	NaN	NaN	NaN	2.1×10 ⁶	8.2×10 ⁵	4.5×10 ⁶
April	3.8×10 ⁶	2.4×10 ⁶	5.4×10 ⁶	4.9×10 ⁶	3.6×10 ⁶	8.1×10 ⁶	3.7×10 ⁶	2.4×10 ⁶	5.4×10 ⁶
May	4.2×10 ⁶	2.6×10 ⁶	6.1×10 ⁶	7.4×10⁶	4.7×10 ⁶	1.1×10 ⁷	5.5×10 ⁶	3.3×10 ⁶	7.6×10 ⁶
June	6.2×10 ⁶	3.7×10 ⁶	1.0×10 ⁷	5.9×10 ⁶	4.2×10 ⁶	9.4×10 ⁶	3.9×10 ⁶	2.1×10 ⁶	5.7×10 ⁶
July	4.1×10 ⁶	2.0×10 ⁶	6.6×10 ⁶	3.5×10 ⁶	1.7×10 ⁶	6.3×10 ⁶	2.6×10 ⁶	1.7×10 ⁶	4.0×10 ⁶
August	3.6×10 ⁶	1.9×10 ⁶	9.5×10 ⁶	5.3×10 ⁶	3.3×10 ⁶	8.1×10 ⁶	3.6×10 ⁶	2.2×10 ⁶	5.4×10 ⁶
September	7.2×10 ⁶	5.2×10 ⁶	9.8×10 ⁶	5.0×10 ⁶	2.6×10 ⁶	8.3×10 ⁶	NaN	NaN	NaN
October	4.5×10 ⁶	2.4×10 ⁶	6.8×10 ⁶	3.4×10 ⁶	2.4×10 ⁶	5.1×10 ⁶	3.0×10 ⁶	2.0×10 ⁶	4.5×10 ⁶
November	2.9×10 ⁶	2.1×10 ⁶	4.8×10 ⁶	2.5×10 ⁶	1.7×10 ⁶	3.6×10 ⁶	2.1×10 ⁶	6.3×10 ⁵	6.0×10 ⁶
December	2.8×10 ⁶	1.6×10 ⁶	4.6×10 ⁶	2.0×10⁶	1.6×10 ⁶	2.4×10 ⁶	NaN	NaN	NaN

221

Typical nighttime sulfuric acid concentration of urban Beijing ranges from 1.6×10^5 to 6.3×10^5 molec cm⁻³

222

(monthly median concentration, Figure S3 and Table S2), about one order of magnitude lower than that of daytime.

223

Unlike daytime sulfuric acid, nighttime sulfuric acid concentration does not show a decreasing trend from 2019 to

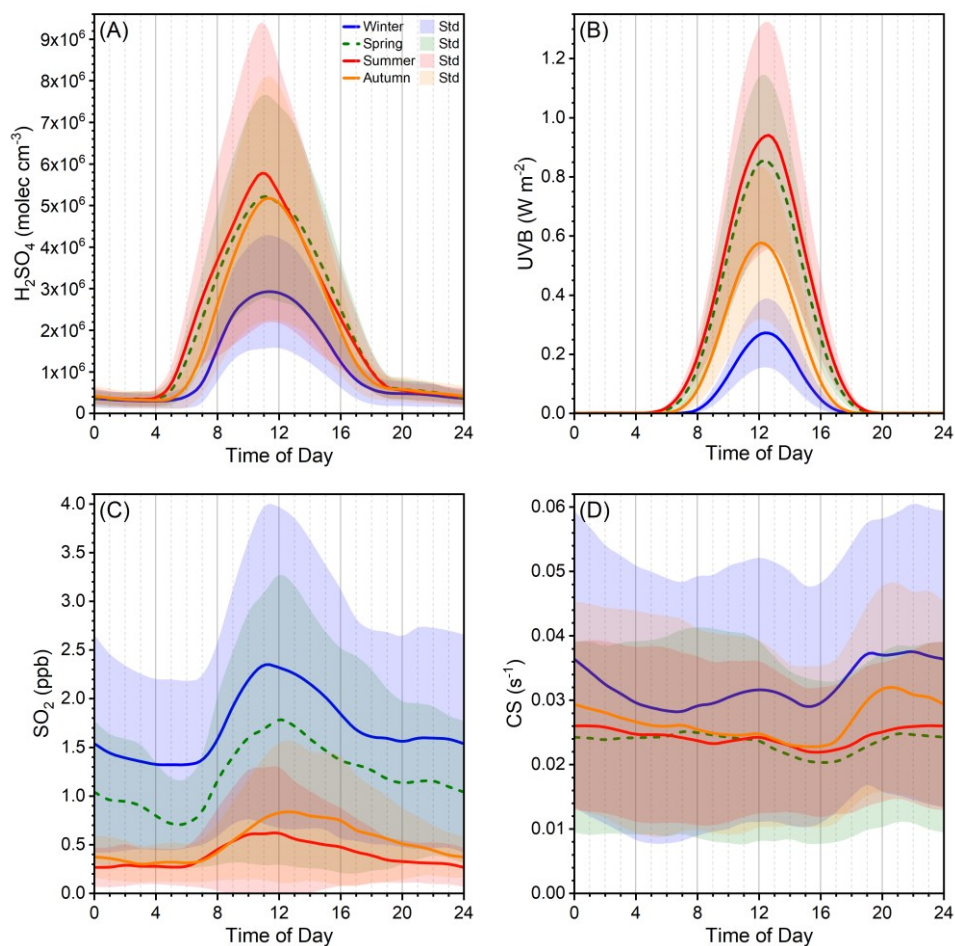
224 2021. At night, under clean conditions, alkene ozonolysis is a major source of sulfuric acid (Guo et al., 2021); under
225 more polluted conditions, primary emissions from vehicles or fresh plumes indicated by benzene also play an
226 important role (Yang et al., 2021a). However, data of alkenes and benzene is unavailable in July–August 2019 and
227 in 2020–2021, making it impossible to estimate the intensities of these nocturnal sulfuric acid sources. Thus, we are
228 not able to give further explanation on the yearly variation of nighttime sulfuric acid. Figure S3A shows that
229 nighttime sulfuric acid has a similar but weaker seasonal variation as that of daytime, i.e., concentration is generally
230 higher from May to September than in other months, and concentration in July and August is significantly lower
231 than in May, June and September. According to the data of 2019, the direct-emission source is higher from March
232 to June (Figure S3B), and alkene-ozonolysis source is higher from March to September (Figure S3C), indicating
233 that the sources of nighttime sulfuric acid are stronger in warmer seasons. Meanwhile, the CS level is lower from
234 April to October (Figure S3D), resulting in lower losses of sulfuric acid. Together, these two factors lead to higher
235 nighttime sulfuric acid concentrations during warmer seasons.

236 **3.1.2 Diurnal variations of sulfuric acid and related parameters**

237 The diurnal patterns of sulfuric acid across seasons are similar, starting increasing in the early morning (~ 04:00–
238 06:00), peaking around noon (~ 11:00), and decreasing to a low level at nightfall (~19:00) (Figure 2A). The morning
239 increase of sulfuric acid occurs earliest in summer, followed by spring, autumn and winter. Moreover, the peak
240 width of sulfuric acid from the widest to narrowest follows the same seasonal trend. These diurnal patterns across
241 the four seasons resemble those of UVB (Figure 2B), suggesting that radiation-driven photochemical reactions
242 govern sulfuric acid formation. Moreover, the morning increase of sulfuric acid occurs earlier than UVB and global
243 radiation but close to $J(\text{NO}_2)$ and OH radical (Figure S4D). This suggests that UVB and global radiation are not
244 able to adequately represent the photochemical sources in early morning, whereas SO_2 oxidation by OH radical
245 produced by NO_2 photolysis is a major source. HONO photolysis is another major formation pathway for OH radical
246 (Tan et al., 2017; Tan et al., 2018; Ma et al., 2019; Yang et al., 2021b; Ma et al., 2022). HONO decreases in the
247 morning at ~ 06:00–07:00, more than an hour after the morning increase of sulfuric acid and OH radical (Figure
248 S4D). This suggests that sulfuric acid formation in the early morning is not likely caused by the oxidation of OH
249 radical from HONO photolysis. The daytime peaking hour of sulfuric acid is close to $J(\text{NO}_2)$ and $J(\text{O}^1\text{D})$ (Figure
250 S4B), indicating that sulfuric acid peaking hour is controlled by photochemical reactions related to $J(\text{NO}_2)$ and
251 $J(\text{O}^1\text{D})$. The peak width of sulfuric acid is the widest, followed by $J(\text{NO}_2)$, global radiation, OH radical, $J(\text{O}^1\text{D})$ and
252 UVB (Figure S4C). This implies that when using proxies with these parameters to estimate daytime sulfuric acid
253 concentration, differences in peaking hours and peak widths may cause deviations from the measured concentration.

254 During the day, sulfuric acid concentration is the highest in summer, followed by spring and autumn, and then
255 winter. This seasonal variation generally tracks UVB, except in autumn, when UVB and SO_2 are lower than spring,
256 but daytime sulfuric acid concentration remains comparable to that in spring. In autumn, the frequency of sulfuric
257 acid with high concentrations ($\geq 1.2 \times 10^7$ molec cm^{-3}) is higher than spring (Figure S5), likely contributing to the
258 overall higher level of sulfuric acid. At night, sulfuric acid concentrations are comparable across seasons, even

259 though SO₂ and CS levels vary. As aforementioned, additional sources such as benzene-related emissions (Yang et
 260 al., 2021a) are among the main nighttime sources of sulfuric acid, so nighttime sulfuric acid cannot be easily
 261 interpreted by proxies only including SO₂, CS and OH radical.



262

263

264

265

266

267

Figure 2. Three-year (from 2019 to 2021) diurnal variations of (A) H₂SO₄, (B) UVB, (C) SO₂ and (D) condensation sink (CS). Winter, spring, summer and autumn periods cover 15th November to 15th March of next year, 16th March to May, June to August, and September to 14th November, respectively. Lines are the mean values, and shaded areas denote the standard deviations of the data.

268

3.2 Performance of sulfuric acid proxies from previous study

269

270

271

272

273

274

275

276

277

278

In previous studies, several representative proxies for sulfuric acid that incorporate real physical and chemical considerations have been proposed. Before constructing the proxy for this study, we first evaluate the performance of existing proxies on estimating sulfuric acid concentration. The equations and internal parameters of these nine proxies are listed in Table 3 (Petäjä et al., 2009;Mikkonen et al., 2011;Lu et al., 2019;Dada et al., 2020). Figure 3 shows the measured sulfuric acid concentration and the proxy-estimated concentrations during daytime (10:00–14:00) in 2019. Table S3 summarizes the corresponding mean, standard deviation, median, lower quartile and upper quartile of sulfuric acid concentrations. To have a more accurate understanding on proxy performance, the correlation coefficients, power exponents, and slopes of the linear fittings between measured and estimated sulfuric acid, as well as the relative errors of estimated to measured sulfuric acid concentrations are further evaluated (Table 4). The relative error is calculated as follows (Lu et al., 2019):

279

$$RE = \frac{1}{n} \cdot \sum_{i=1}^n \frac{|[H_2SO_4]_{pro,i} - [H_2SO_4]_{mea,i}|}{[H_2SO_4]_{mea,i}} \quad (9)$$

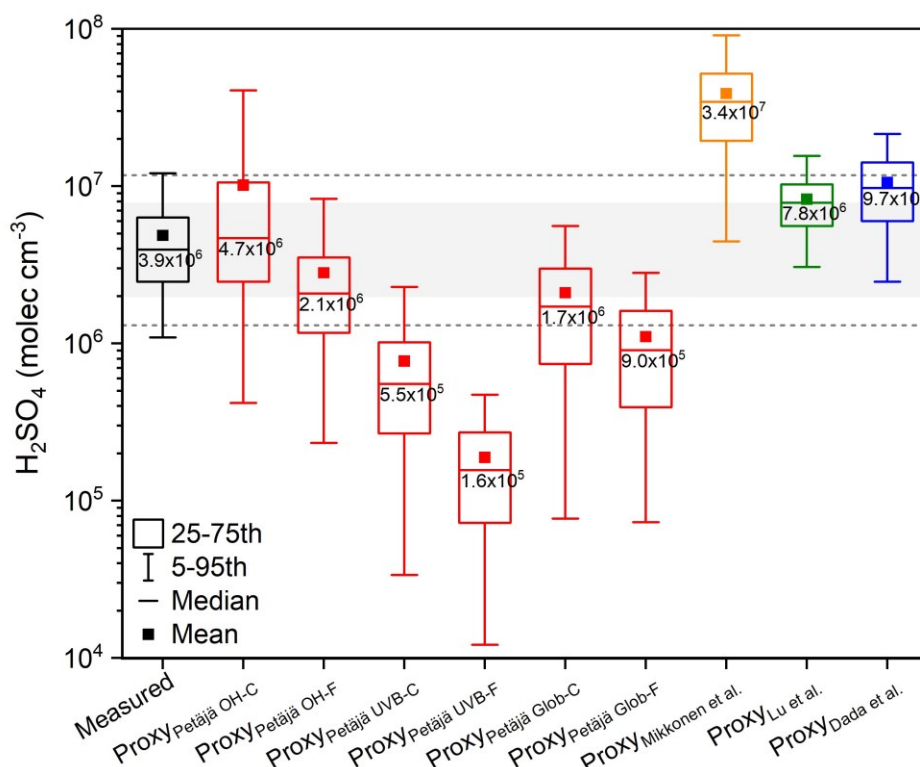
280 **Table 3.** The equations and internal parameters of nine sulfuric acid proxies from literatures.

Proxy	Equation	Parameters	Reference
Proxy _{Petäjä OH-C}	$P_1 = \frac{k_1 \cdot [SO_2] \cdot [OH]}{CS}$	$k_1 = 2.2 \times 10^{-12} \text{ cm}^3 \text{ molec}^{-1} \text{ s}^{-1}$	
Proxy _{Petäjä OH-F}		$k_1 = 8.6 \times 10^{-10} \times [OH]^{-0.48} \text{ cm}^3 \text{ s}^{-1}$	
Proxy _{Petäjä UVB-C}	$P_2 = \frac{k_2 \cdot [SO_2] \cdot UVB}{CS}$	$k_2 = 9.9 \times 10^{-7} \text{ m}^2 \text{ W}^{-1} \text{ s}^{-1}$	(Petäjä et al., 2009)
Proxy _{Petäjä UVB-F}		$k_2 = 8.4 \times 10^{-7} \times UVB^{-0.68} \text{ m}^2 \text{ W}^{-1} \text{ s}^{-1}$	
Proxy _{Petäjä Glob-C}	$P_3 = \frac{k_3 \cdot [SO_2] \cdot Glob}{CS}$	$k_3 = 2.3 \times 10^{-9} \text{ m}^2 \text{ W}^{-1} \text{ s}^{-1}$	
Proxy _{Petäjä Glob-F}		$k_3 = 1.4 \times 10^{-7} \times Glob^{-0.70} \text{ m}^2 \text{ W}^{-1} \text{ s}^{-1}$	
Proxy _{Mikkonen et al.}	$a \cdot k \cdot \text{Radiation}^b \cdot [SO_2]^c \cdot (CS \cdot RH)^f$	$a = 8.21 \times 10^{-3}, b = 1,$ $c = 0.62, f = -0.13$	(Mikkonen et al., 2011)
Proxy _{Lu et al.}	$k_0 \cdot UVB^a \cdot [SO_2]^b \cdot CS^c \cdot (O_3^d + NO_x^f)$	$k_0 = 0.0013, a = 0.13, b = 0.40,$ $c = -0.17, d = 0.44, f = 0.41$	(Lu et al., 2019)
Proxy _{Lubna et al.}	$-\frac{CS}{2k_3} + \sqrt{\left(\frac{CS}{2k_3}\right)^2 + \frac{[SO_2]}{k_3}} \cdot k_1 \cdot Glob$	$k_1 = 1.0 \times 10^{-6}, k_3 = 1.6 \times 10^{-7}$	(Dada et al., 2020)

281 As shown in Figure 3 and Table 4, estimated sulfuric acid concentrations from Proxy_{Petäjä OH-C}, Proxy_{Petäjä OH-F}
282 and Proxy_{Lu et al.} are closest to the measured one, with median deviations within twofold. This suggests that these
283 three proxies provide the best estimates of sulfuric acid concentration. Estimated sulfuric acid concentrations from
284 Proxy_{Petäjä Glob-C} and Proxy_{Dada et al.} are not too far away from the measured one, with median deviations within
285 threefold. While estimated concentrations from other proxies differ substantially from the measured one, especially
286 Proxy_{Petäjä UVB-F}, which underestimates sulfuric acid concentration markedly. The linear correlation coefficients of
287 Proxy_{Petäjä OH-C}, Proxy_{Petäjä OH-F} and Proxy_{Petäjä UVB-C} proxies are closet to 1.0. Similarly, the power exponents of
288 Proxy_{Petäjä OH-C}, Proxy_{Petäjä OH-F}, Proxy_{Petäjä UVB-C} and Proxy_{Petäjä Glob-C} are closet to 1.0. This indicates that the estimated
289 sulfuric acid from former three proxies have the best linear correlation with the measurement. Only the slope of
290 Proxy_{Petäjä OH-C} (0.85) is close to 1.0, suggesting that it performs the best in linear relationship. For Proxy_{Petäjä UVB-F},
291 Proxy_{Petäjä Glob-F}, Proxy_{Mikkonen et al.}, Proxy_{Lu et al.} and Proxy_{Dada et al.}, none of the linear correlation coefficients, power
292 exponents or the slopes perform well, indicating that they fail to reproduce the linearity with measured sulfuric acid.
293 The relative errors are within 50% for Proxy_{Petäjä OH-F}, Proxy_{Petäjä Glob-C} and Proxy_{Petäjä Glob-F}, and those for Proxy_{Petäjä}
294 OH-C, Proxy_{Petäjä UVB-C}, Proxy_{Petäjä UVB-F} and Proxy_{Lu et al.} range from 57% to 91%.

295 Considering both linear correlation and concentration estimation accuracy, Proxy_{Petäjä OH-C} and Proxy_{Petäjä OH-F} are
296 the two most suitable proxies for reproducing sulfuric acid concentration. Other four proxies from Petäjä et al., 2009
297 without the OH radical term underestimate the concentration of sulfuric acid. The reason might be that the scaling
298 factors k_2 and k_3 were obtained by fitting measured sulfuric acid and other parameters rather than deriving from the
299 direct relationships between UVB/global radiation and OH radical. Under this circumstance, scaling factors k_2 and
300 k_3 are influenced by measured sulfuric acid, UVB and global radiation as well as calculated CS, which may
301 introduce substantial uncertainties. Moreover, for both concentration estimation and linearity (R, exponent and
302 linear slope), proxies with fitted scaling factors performed worse than those with constant scaling factors. This may

303 be due to the absence of linear relationships between proxies and photochemical terms (OH radical, UVB, or global
 304 radiation), since the fitted scaling factors k_1 , k_2 and k_3 all include the photochemical term (Table 3).



305
 306 **Figure 3.** Sulfuric acid concentrations from measurement and estimated by proxies from literatures during the time window of
 307 10:00-14:00 in 2019 (1st January to 31st December). Black value inside each box is the median concentration. “Proxy_{Petäjä} OH-
 308 C” “Proxy_{Petäjä} OH-F” “Proxy_{Petäjä} UVB-C” “Proxy_{Petäjä} UVB-F” “Proxy_{Petäjä} Glob-C” and “Proxy_{Petäjä} Glob-F” represent sulfuric acid
 309 proxies from the work of Petäjä et al., 2009, with P₁ proxy using OH radical with constant pre-factor k_1 , P₁ proxy using OH
 310 radical with fitted pre-factor k_1 , P₂ proxy using UVB with constant pre-factor k_2 , P₂ proxy using UVB with fitted pre-factor k_2 ,
 311 P₃ proxy using global radiation with constant pre-factor k_3 , and P₃ proxy using global radiation with fitted pre-factor k_3 ,
 312 respectively. “Proxy_{Mikkonen et al.}” “Proxy_{Lu et al.}” and “Proxy_{Dada et al.}” are sulfuric acid proxies from the work of Mikkonen et al.
 313 2011, Lu et al. 2019 and Dada et al. 2020, respectively. Gray area covers 50% to 200% of median concentration of measured
 314 sulfuric acid, and two gray lines cover 33.3% to 300% of median concentration of measured sulfuric acid.

315 **Table 4.** The correlation coefficients (R), power exponents (Exponent) and slopes (Linear Slope) of the linear fittings between
 316 measured sulfuric acid concentration and the estimated ones using proxies from literatures, the relative errors (RE) of the
 317 estimated sulfuric acid concentrations to the measured one, as well as the ratios of proxy concentrations to measured
 318 concentration using mean ($[\text{Proxy}/\text{Measured}]_{\text{mean}}$) and median ($[\text{Proxy}/\text{Measured}]_{\text{median}}$) values. All parameters are fitted with
 319 Bisquare fitting.

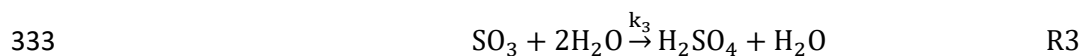
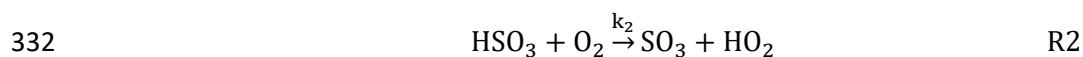
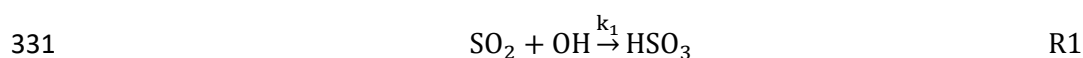
Proxy	R	Exponent	Linear Slope	RE (%)	$[\text{Proxy}/\text{Measured}]_{\text{mean}}$	$[\text{Proxy}/\text{Measured}]_{\text{median}}$	References
Proxy _{Petäjä} OH-C	0.97	1.17	0.85	74 %	2.09	1.18	(Petäjä et al., 2009)
Proxy _{Petäjä} OH-F	0.78	0.80	0.30	35 %	0.58	0.53	
Proxy _{Petäjä} UVB-C	0.84	1.08	0.09	57 %	0.16	0.14	
Proxy _{Petäjä} UVB-F	0.52	0.63	0.01	64 %	0.04	0.04	
Proxy _{Petäjä} Glob-C	0.59	0.86	0.16	40 %	0.43	0.43	
Proxy _{Petäjä} Glob-F	0.44	0.57	0.05	50 %	0.23	0.23	
Proxy _{Mikkonen et al.}	0.46	0.49	2.40	565 %	7.98	8.70	(Mikkonen et al., 2011)
Proxy _{Lu et al.}	0.38	0.30	0.42	91 %	1.70	1.99	(Lu et al., 2019)
Proxy _{Dada et al.}	0.18	0.30	0.45	133 %	2.17	2.46	(Dada et al., 2020)

320

321 Note that the scaling factor k_1 of the OH-based proxy was obtained by replacing the left hand side of the equation
 322 with measured sulfuric acid concentration (Petäjä et al., 2009). Thus, k_1 was not derived from the chemical
 323 production pathways of sulfuric acid, and the best-fit value of k_1 may vary from site to site. This limitation restricts
 324 its applicability across a broader range of sites. Therefore, in this study, we aim to derive a proxy based entirely on
 325 the formation and loss pathways of sulfuric acid, where the parameters, related pre-factors and exponents all have
 326 chemical and physical meanings. Proxies of this kind should be applicable across different sites, since no site-
 327 dependent scaling factors or exponents are used.

328 3.3 Derivation of sulfuric acid proxies from its budget analysis

329 During daytime, the main formation pathway of sulfuric acid is the SO_2 oxidation by OH radical, followed by
 330 O_2 and H_2O addition (R1–R3) (Finlayson-Pitts and Pitts Jr., 2000):



334 As OH radical oxidation is the rate-limiting step, the production rate of sulfuric acid is nearly equivalent to that of
 335 HSO_3 and can be calculated as follows:

$$336 \quad P_{[\text{H}_2\text{SO}_4]} = P_{[\text{HSO}_3]} = k_1 \cdot [\text{SO}_2] \cdot [\text{OH}] \quad (10)$$

337 Regarding sulfuric acid losses, the main loss pathway is its condensation sink onto particle surfaces (Dada et al.,
 338 2020;Guo et al., 2021;Yang et al., 2021a), which can be written as:

$$339 \quad L_{[\text{H}_2\text{SO}_4]} = [\text{H}_2\text{SO}_4] \cdot \text{CS} \quad (11)$$

340 The production and loss rates of sulfuric acid are much faster than its net concentration change (Guo et al., 2021),
 341 so a pseudo-steady-state assumption can be applied:

$$342 \quad k_1 \cdot [\text{SO}_2] \cdot [\text{OH}] \approx [\text{H}_2\text{SO}_4] \cdot \text{CS} \quad (12)$$

343 Then, the steady-state concentration of sulfuric acid can be estimated, which can be called as the OH-CS based
 344 proxy:

$$345 \quad \text{Proxy}_{\text{OH,CS}} = [\text{H}_2\text{SO}_4] = \frac{k_{\text{SO}_2\text{-OH}} \cdot [\text{SO}_2] \cdot [\text{OH}]}{\text{CS}} \quad (13)$$

346 Here, $k_{\text{SO}_2\text{-OH}}$ is the rate constant of SO_2 oxidation by OH radical. It is taken as $1.3 \times 10^{-12} (T/300)^{-0.7} \text{ cm}^3 \text{ s}^{-1}$, where
 347 T is the temperature in Kelvin (Wine et al., 1984;Atkinson et al., 2004), $[\text{SO}_2]$ and $[\text{OH}]$ are concentrations of SO_2
 348 and OH radical in molec cm^{-3} , and CS is condensation sink of sulfuric acid in s^{-1} . Compared with the proxy proposed
 349 by Petäjä et al. (2009), the pre-factor $k_{\text{SO}_2\text{-OH}}$ is not obtained by parameter fitting but is a verified reaction
 350 coefficient derived from experiments. Therefore, this proxy is chemically meaningful and has the potential to be
 351 used at various sites.

352 It is widely acknowledged that the OH radical is difficult to measure. Therefore, for most sites lacking OH
 353 radical measurements, the OH-CS based proxy cannot be applied. A major production pathway for OH radical is

354 the photolysis of NO₂ and O₃, along with radical recycling (Lu et al., 2012;Ma et al., 2022), all driven by solar
 355 radiation (Rohrer and Berresheim, 2006). Thus, UVB, a readily available parameter, can replace [OH] in Eq. (13)
 356 to derive the second proxy as follows:

$$357 \quad \text{Proxy}_{\text{UVB,CS}} = \frac{k_{\text{UVB-CS}} \cdot [\text{SO}_2] \cdot \text{UVB}}{\text{CS}} \quad (14)$$

358 where $k_{\text{UVB-CS}}$ is the pre-factor, and [SO₂], UVB, and CS are in the units of molec cm⁻³, W m⁻² and s⁻¹, respectively.
 359 As shown in Figure S7A, OH radical and UVB has a linear correlation with R value of 0.86. The ratio of OH radical
 360 to UVB is 6.14×10^6 molec cm⁻³ W⁻¹ m². Accounting for this ratio yields $k_{\text{UVB-CS}}$ of 7.98×10^{-6} (T/300)^{-0.7} W⁻¹ m²
 361 s⁻¹. Replacing the left hand side of Eq. (14) with measured sulfuric acid concentration yields $k_{\text{UVB-CS}}$ of 7.5×10^{-6}
 362 (T/300)^{-0.7} W⁻¹ m² s⁻¹, which is close to the value derived from the OH-UVB relationship. This $k_{\text{UVB-CS}}$ is finally
 363 used as it brings less deviation between measured and estimated sulfuric acid concentrations.

364 Furthermore, calculating CS requires particle size distribution data, which is not always available. In this case,
 365 a surrogate parameter for CS is needed. The condensation sink of gaseous species onto particles is mainly
 366 determined by the aerosol surface area. PM_{2.5} measures the masses of particles. In principle, CS and PM_{2.5} should
 367 follow a power-law relationship with an exponent of 2/3. As expected, PM_{2.5}^{2/3} and CS are well linearly correlated
 368 (Figure S7B, R=0.92). Thus, replacing CS in Eq. (14) with PM_{2.5}^{2/3} yields the third proxy as follows:

$$369 \quad \text{Proxy}_{\text{UVB,PM}_{2.5}} = \frac{k_{\text{UVB-PM}_{2.5}} \cdot [\text{SO}_2] \cdot \text{UVB}}{\text{PM}_{2.5}^{2/3}} \quad (15)$$

370 where $k_{\text{UVB-PM}_{2.5}}$ is the pre-factor, and [SO₂], UVB, and PM_{2.5} are in the units of molec cm⁻³, W m⁻² and μg m⁻³,
 371 respectively. The slope of CS to PM_{2.5}^{2/3} is 2.67×10^{-3} s⁻¹ μg^{-2/3} m². Then, substituting [OH] with UVB and CS with
 372 PM_{2.5}^{2/3} yields $k_{\text{UVB-PM}_{2.5}}$ of 2.99×10^{-3} μg^{2/3} W⁻¹. Replacing the left hand side of Eq. (15) with measured sulfuric
 373 acid concentration yields $k_{\text{UVB-PM}_{2.5}}$ of 2.8×10^{-3} μg^{2/3} W⁻¹, which is close to the value derived from the OH-UVB
 374 and CS-PM_{2.5} relationships and is finally used.

375 We summarize the three proxies incorporating the corresponding parameters as follows:

$$376 \quad \text{Proxy}_{\text{OH,CS}} = (1.3 \times 10^{-12}) \times \left(\frac{T}{300}\right)^{-0.7} \times [\text{SO}_2] \times [\text{OH}] \div \text{CS} \quad (16)$$

$$377 \quad \text{Proxy}_{\text{UVB,CS}} = (7.5 \times 10^{-6}) \times \left(\frac{T}{300}\right)^{-0.7} \times [\text{SO}_2] \times \text{UVB} \div \text{CS} \quad (17)$$

$$378 \quad \text{Proxy}_{\text{UVB,PM}_{2.5}} = (2.8 \times 10^{-3}) \times [\text{SO}_2] \times \text{UVB} \div \text{PM}_{2.5}^{2/3} \quad (18)$$

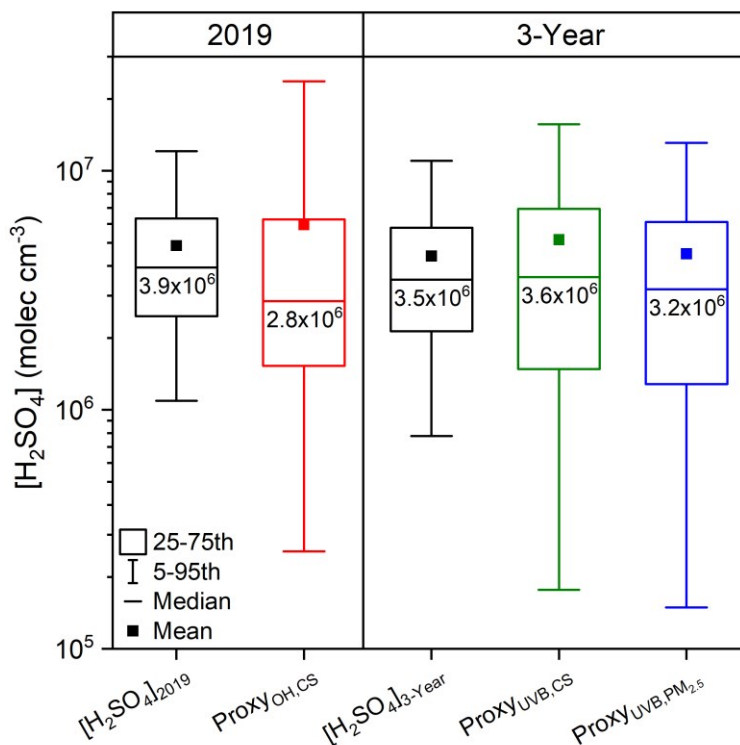
379 The uncertainties of the OH-CS, UVB-CS, and UVB-PM_{2.5} based proxies, based on Eqns. (16–18), are estimated
 380 to be 41.7%, 96.1%, and 100.4%, respectively. Details are provided in Section S3.

381 **3.4 Evaluation of different sulfuric acid proxies in this study**

382 **3.4.1 Performance of sulfuric acid proxies at Beijing Site**

383 Figure 4 shows the overall concentrations of measured and estimated sulfuric acid from proxies. The estimated
 384 sulfuric acid concentrations from three proxies are generally in good agreement with the measured one, although
 385 the OH-CS-based proxy yields slightly lower concentration than measurement. Additionally, the concentration

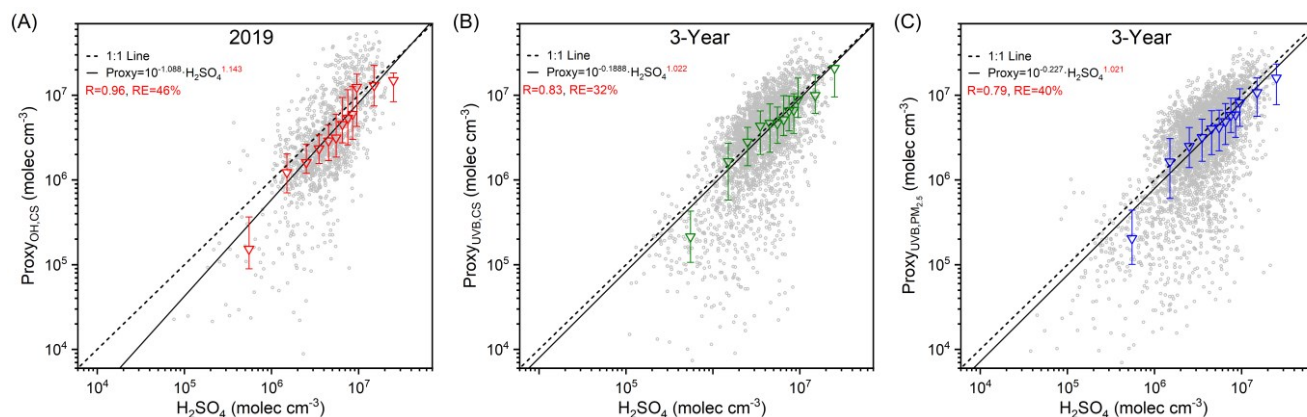
386 ranges estimated by proxies are broader than the measured one. Detailed sulfuric acid concentrations, including
 387 mean, standard deviation, median, lower quartile and upper quartile values are summarized in Table S4.



388 **Figure 4.** Sulfuric acid concentrations from measurement and estimated by proxies in this study during daytime (10:00-14:00).
 389

390 The scatter plots of three proxies vs. measured sulfuric acid are shown in Figure 5. For all three proxies, the
 391 estimated sulfuric acid concentrations are well correlated with the measured one, with most data points falling on
 392 or near the 1:1 line. This suggests that the three steady-state based proxies generally perform well in estimating
 393 daytime sulfuric acid concentration. However, slight deviations between the least-square-fit lines and the 1:1 lines
 394 can be observed. To better understand these deviations, we summarize the correlation coefficients and power
 395 exponents of the fits between measured and estimated sulfuric acid concentrations, as well as the relative errors of
 396 the estimated concentrations (Table 5). The OH-CS-based proxy shows the best correlation ($R = 0.96$). The R values
 397 for the UVB-CS based proxy (0.83) and the UVB-PM_{2.5} based proxy (0.79) are also close to unity. The OH-CS
 398 based proxy has an exponent of 1.14, indicating that the relationship between proxy and measured sulfuric acid is
 399 not strictly linear, which could, to some extent, arise from the uncertainty in OH radical modelling. The exponents
 400 of UVB-CS based proxy (1.02) and UVB-PM_{2.5} based proxy (1.02) are very close to 1.0, suggesting excellent good
 401 linear relationships between proxies measured sulfuric acid. The relative errors of three proxies are all within 50%,
 402 which performs better than most proxies from previous studies (Table 4). Moreover, the ratios of proxy to measured
 403 concentrations give the same result that they are in the range of 0.72–1.22, much closer to 1.0 than most proxies
 404 from previous studies (Table 4). It should be pointed out that, as the time window moves further from noon, the
 405 OH-CS based proxy increasingly underestimates the sulfuric acid concentration. And as the time window shifts
 406 away from noon, the relationship between proxy and measured sulfuric acid becomes increasingly nonlinear. This

407 implies that in the early morning or at nightfall, sulfuric acid sources other than OH+SO₂ pathway cannot be
 408 neglected (Figure S15).



409
 410 **Figure 5.** Sulfuric acid concentrations estimated by proxies in this study vs. the measured concentration during daytime (10:00-
 411 14:00) for (A) OH-CS based proxy in 2019, (B) UVB-CS based proxy in 3 years, and (C) UVB-PM_{2.5} based proxy in 3 years.
 412 The black dashed lines are 1:1 lines, and the black lines are the distance weighted least square fits between proxy and measured
 413 sulfuric acid. Corresponding functions of the fits, correlation coefficients (R) and relative errors (RE) are shown in the legend.
 414 The triangle marker represents the binned data, where the up line, middle marker and bottom lines stand for upper quartile,
 415 median and lower quartile, respectively.

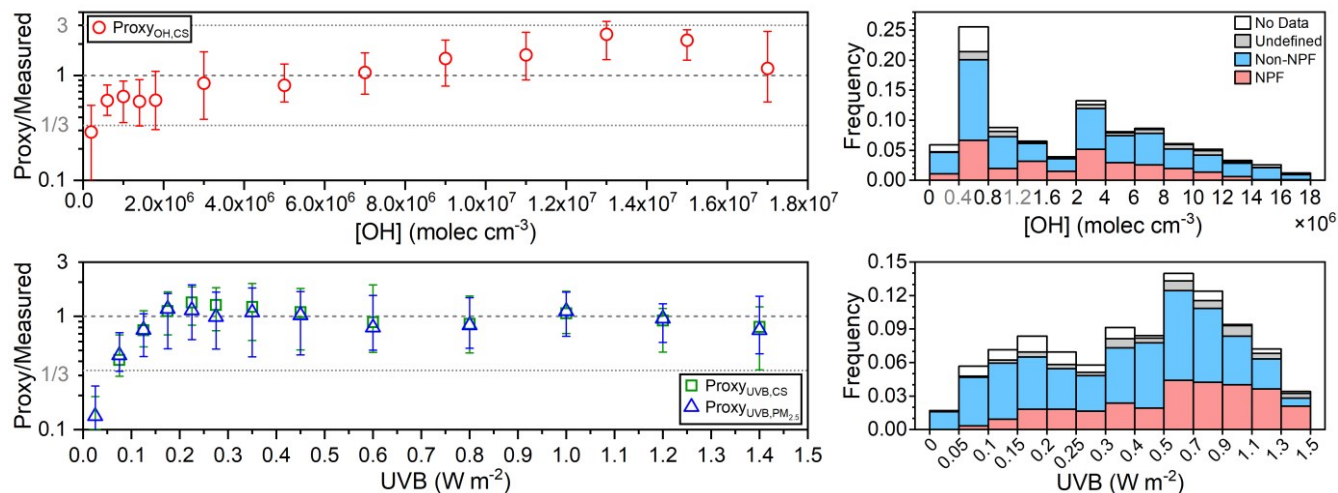
416 **Table 5.** The correlation coefficients (R) and power exponents (Exponent) of the linear fittings between measured sulfuric acid
 417 concentration and the estimated ones using proxies in this study, the relative errors (RE) of the estimated sulfuric acid
 418 concentrations to the measured one, as well as the ratios of proxy concentrations to measured concentration using mean
 419 ([Proxy/Measured]_{mean}) and median ([Proxy/Measured]_{median}) values.

Year	Parameters	R	Exponent	RE (%)	[Proxy/Measured] _{mean}	[Proxy/Measured] _{median}
2019	Proxy _{OH,CS}	0.96	1.14	46%	1.22	0.72
3-Year	Proxy _{UVB,CS}	0.83	1.02	32%	1.17	1.03
	Proxy _{UVB,PM_{2.5}}	0.79	1.02	40%	1.02	0.91

420 To have better understanding on the performance of sulfuric acid proxies at any given moment, the time
 421 variations of sulfuric acid concentrations from three proxies and measurement are shown in Figures S8 and S9.
 422 Generally, the OH-CS based proxy provides a good estimation on daytime sulfuric acid concentration (Figure S8).
 423 Specifically, in 2019, the concentration estimated by this proxy matches well with the measured one in January,
 424 February, March, April, August, and September. In other months of 2019, it underestimates or overestimates
 425 sulfuric acid concentration. This shows that although the OH-CS-based proxy generally performs well, sulfuric acid
 426 concentration at a given moment may deviate. Similarly, sulfuric acid concentrations estimated by UVB-CS based
 427 and UVB-PM_{2.5} based proxies generally match well with the measured one at most of the daytime, with deviations
 428 noticeable in several months over 3 years (Figures S8 and S9). These time variations are consistent with the findings
 429 in Section 3.1.2: the daily peak width of OH-CS based proxy is narrower than that of measured sulfuric acid, and
 430 the daily peak widths of UVB-CS based and UVB-PM_{2.5} based proxies are narrower than that of OH-CS based
 431 proxy. Furthermore, the OH-CS based proxy partially reproduces the formation of sulfuric acid at night and early
 432 morning, with evidence on most days of January 2019 and some days of February 2019. Although UVB-CS based
 433 and UVB-PM_{2.5} based proxies cannot estimate nighttime sulfuric acid, they provide a convenient, reliable and, more
 434 importantly, feasible way to trace the long-term daytime sulfuric acid concentration for sites without OH radicals.

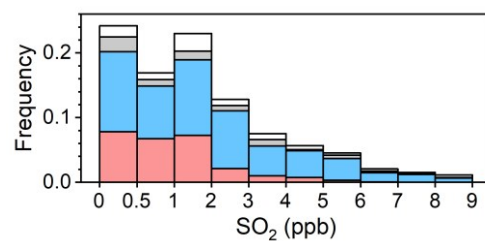
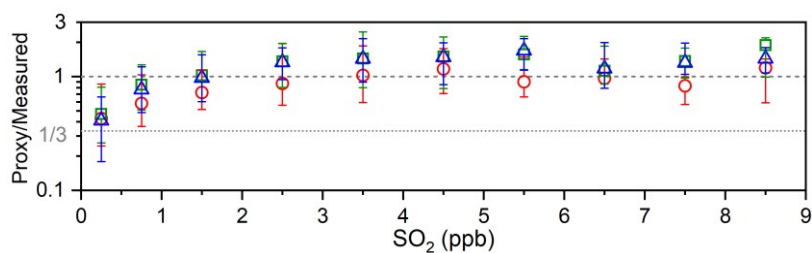
435 Sulfuric acid concentration is estimated using OH radical, UVB, SO₂, CS and PM_{2.5}. We then use these
 436 parameters to assess how well the proxy-estimated concentrations match the measured values, and to determine the
 437 applicable parameter ranges of the proxies. Figure 6 shows that when [OH] is lower than 4×10⁵ molec cm⁻³, UVB
 438 is lower than 0.10 W m⁻² or SO₂ is lower than 0.5 ppb, all three steady-state based proxies underestimate sulfuric
 439 acid concentration. This suggests that when the OH radical, UVB, or SO₂ is low, other SO₂ oxidation pathways or
 440 additional sulfuric acid sources contribute more to sulfuric acid formation. As [OH] increases, the ratio of proxy to
 441 measured sulfuric acid gradually rises above 1.0. These deviations of OH-CS based proxy may arise from
 442 uncertainties in OH radical modelling. As UVB and SO₂ increase, the ratios of proxies to measured sulfuric acid
 443 stabilize around 1.0. This suggests that although the OH-CS based proxy is derived entirely from sulfuric acid
 444 budget analysis, its long-term stability may not be as good as that of UVB-CS based or UVB-PM_{2.5} based proxies,
 445 given the intrinsic uncertainty in OH modeling. The ratio of UVB-CS based proxy stays around 1.0 when CS is
 446 lower than 0.07 s⁻¹, accounting for ~96.3% of total data. Similarly, the ratio of UVB-PM_{2.5} based proxy shows no
 447 clear dependence on PM_{2.5} when it is lower than 200 μg m⁻³, accounting for ~99.6% of all datasets. This indicates
 448 that these two proxies can be applied across almost all CS and PM_{2.5} ranges. For OH-CS based proxy, sulfuric acid
 449 concentration is underestimated when CS is lower than 0.015 s⁻¹ (~32.2%) or higher than 0.07 s⁻¹ (~3.6%). Higher
 450 CS is also associated with more polluted conditions when other sulfuric acid sources such as primary emissions
 451 may exist (Yang et al., 2021a). At lower CS, UVB-CS based proxy performs well, while OH-CS based proxy does
 452 not, suggesting that slightly poor performance of OH-CS based proxy may arise from OH radical modelling.
 453 Meanwhile, the performances of three steady-state based proxies show a clear dependence on RH. When RH is
 454 lower than 60%, the ratios of proxies to measured sulfuric acid stabilize around 1.0. When RH exceeds 60% (~13.6%
 455 of total data), these ratios increase with RH. Higher RH correlates with precipitation events with lower UVB and
 456 lower SO₂, increasing the contribution of additional sulfuric acid sources. This may partly explain the
 457 underestimation of proxies at higher RH.

458

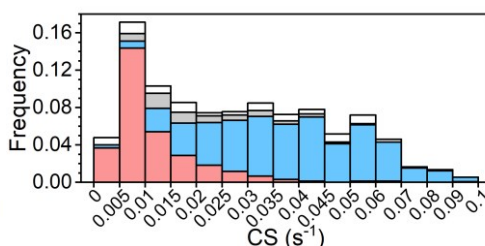
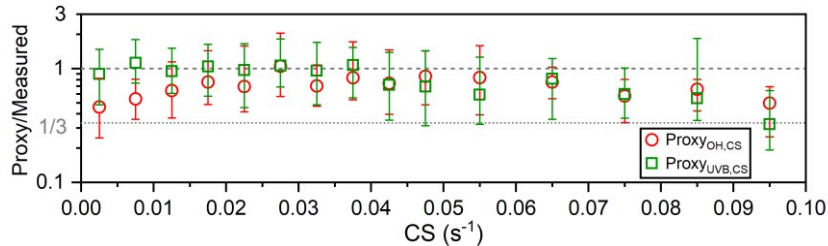


459

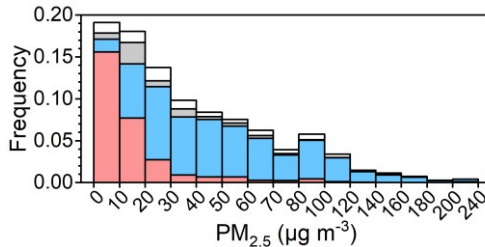
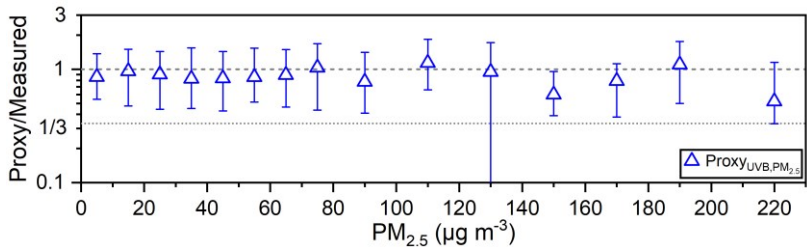
460



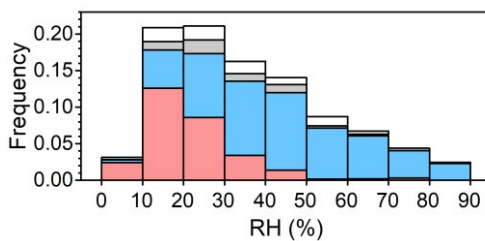
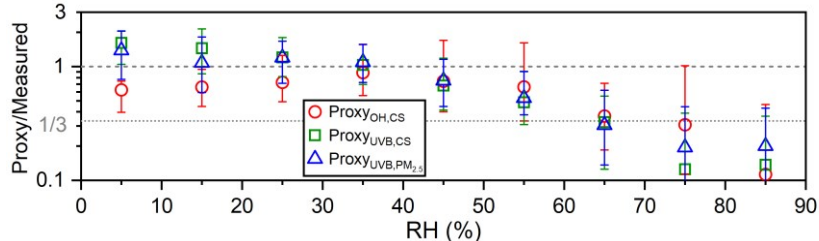
461



462



463



464

465

466

467

468

Figure 6. Left: The ratios of sulfuric acid concentrations estimated by proxies in this study to the measured one (Proxy/Measured) vs. concentration of OH radical ($[\text{OH}]$), UVB, SO_2 , CS, $\text{PM}_{2.5}$ and RH during daytime (10:00-14:00) of 2019. Different colored markers represent different proxies. The up line, middle marker and bottom line stand for upper quartile, median and lower quartile values respectively. Right: Frequency distributions of corresponding parameters classified by “NPF”, “Non-NPF”, “Undefined”, and “No Data” periods.

469

470

471

472

473

474

475

476

477

Sulfuric acid is a key precursor in NPF processes. Therefore, it is necessary to assess how well these proxies perform during NPF periods. As shown in Figures 6 and S10, about 30% of NPF cases fall outside the optimal range of SO_2 , while most NPF cases fall within the optimal ranges of OH radical, UVB, CS, $\text{PM}_{2.5}$, and RH. Consequently, during NPF periods, the performance of three proxies mainly depends on the SO_2 concentration at that time. As shown in Figure S11, restricting the analysis to data within the optimal parameter ranges reduces the number of data points that deviate from the 1:1 line and have extremely low estimated sulfuric acid concentrations. Meanwhile, the correlation coefficients between the estimated and measured sulfuric acid concentrations generally improved, while the relative errors increased, and the improvement in the slopes of linear fits was not significant. This suggests that data outside the optimal parameter ranges generally have little impact on the fitting results.

478

3.4.2 Performance of sulfuric acid proxies at Hyttiälä, Finland

479

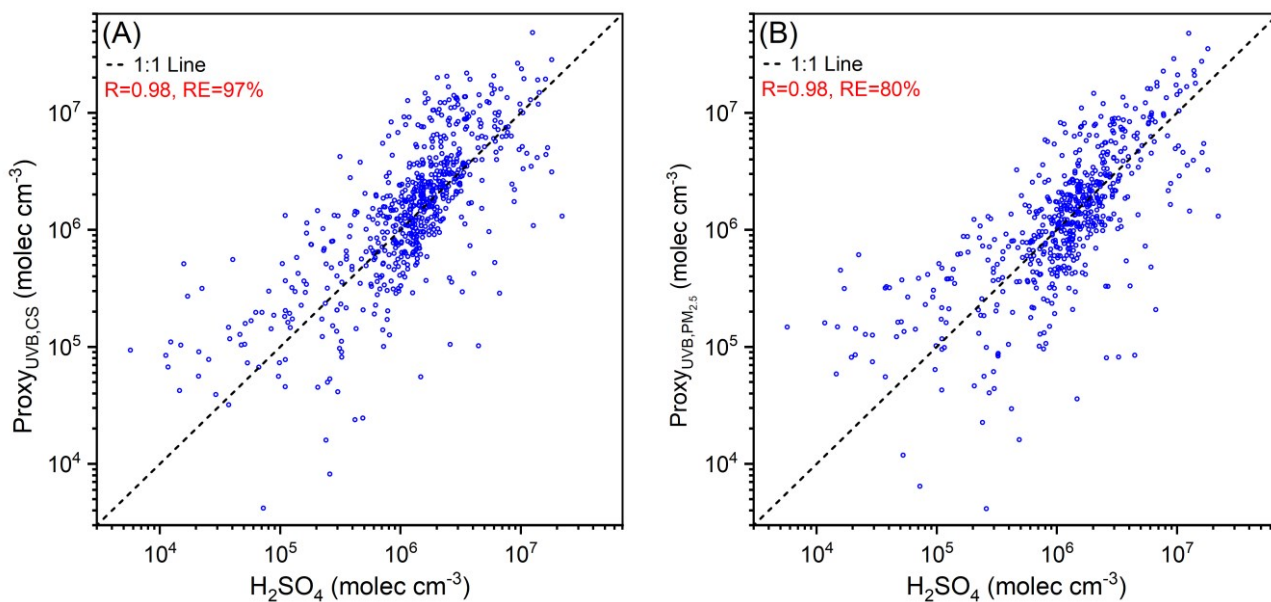
480

Because the three proxies above are derived from the budget analysis of sulfuric acid, Eqns. (16–18) and their pre-factors should be applicable to other sites. To demonstrate this, we use datasets from a boreal forest site in

481 Hyytiälä, Finland as test data. Figure 7 shows the scatter plots of UVB-CS based and UVB-PM_{2.5} based proxies vs.
482 measured sulfuric acid. For both proxies, most data points lie on or are near the 1:1 line, with R values close to 1.0,
483 indicating good linear correlations between the estimated and measured sulfuric acid concentrations. The relative
484 errors for UVB-CS based and UVB-PM_{2.5} based proxies of Hyytiälä site are 97% and 80%, respectively, which are
485 only slightly larger than those of the Beijing site (Table 5) but still within an acceptable range. The above results
486 suggest that both proxies perform well in estimating daytime sulfuric acid concentration at Hyytiälä.

487 For the UVB-CS based proxy, the pre-factor $k_{\text{UVB-CS}}$ in Eq. (17) was chosen the same as Beijing. This proxy
488 estimates sulfuric acid concentrations well at both Beijing and Hyytiälä sites using the same $k_{\text{UVB-CS}}$ value,
489 indicating that the OH-UVB relationships, or the k' values in $[\text{OH}] = k' \cdot \text{UVB}$, do not differ significantly between
490 these two sites. This further suggests that k' values at other sites should not differ significantly, and that $k_{\text{UVB-CS}}$
491 values should be similar across sites.

492 For the UVB-PM_{2.5} based proxy, the pre-factors $k_{\text{UVB-PM}_{2.5}}$ in Eq. (18) are $2.8 \times 10^{-3} \mu\text{g}^{2/3} \text{W}^{-1}$ and $4.7 \times 10^{-3} \mu\text{g}^{2/3}$
493 W^{-1} for Beijing and Hyytiälä, respectively. This difference in $k_{\text{UVB-PM}_{2.5}}$ arises from the disparity of pre-factor in
494 $\text{CS} = k \cdot \text{PM}_{2.5}^{2/3}$, where the values of k are $2.67 \times 10^{-3} \text{s}^{-1} \mu\text{g}^{-2/3} \text{m}^2$ and $1.59 \times 10^{-3} \text{s}^{-1} \mu\text{g}^{-2/3} \text{m}^2$ for Beijing (Figure
495 S7B) and Hyytiälä (Figure S12A), respectively. Specifically, the ratios of 4.7×10^{-3} to 2.8×10^{-3} and of 2.67×10^{-3} to
496 1.59×10^{-3} are both 1.68. Therefore, considering the CS-PM_{2.5} relationships, Eq. (18) is also applicable to Hyytiälä.
497 This tells us that when using the UVB-PM_{2.5} based proxy to estimate sulfuric acid concentration, the k value should
498 be determined first to correct $k_{\text{UVB-PM}_{2.5}}$. Moreover, this coefficient k for one Nanjing site is $1.62 \times 10^{-3} \text{s}^{-1} \mu\text{g}^{-2/3} \text{m}^2$
499 (Figure S16), which falls between those of Beijing and Hyytiälä. This implies that although the values of k vary
500 among sites, this difference remains modest. Figures S8B-C show that the slope of CS to $\text{PM}_{2.5}^{2/3}$ is stable across
501 years and seasons at a given site. Therefore, by conducting short-term synchronous measurement of $\text{PM}_{2.5}$ and
502 particle size distribution, a reliable k can be obtained. In summary, these steady-state based proxies are transferable
503 proxies that can be widely used to estimate daytime sulfuric acid concentration at other atmospheric sites.



504

505 **Figure 7.** (A) UVB-CS based proxy ($\text{Proxy}_{\text{UVB,CS}}$) and (B) UVB- $\text{PM}_{2.5}$ based proxy ($\text{Proxy}_{\text{UVB,PM}_{2.5}}$) vs. measured sulfuric acid
506 of Hyytiälä, Finland during daytime (10:00-14:00) from 8th March to 13th Aug. 2018. The pre-factor of $\text{Proxy}_{\text{UVB,CS}}$ ($k_{\text{UVB,CS}}$)
507 is $7.5 \times 10^{-6} (\text{T}/300)^{-0.7} \text{ W}^{-1} \text{ m}^2 \text{ s}^{-1}$, which is the same as Beijing. The pre-factor of $\text{Proxy}_{\text{UVB,PM}_{2.5}}$ ($k_{\text{UVB,PM}_{2.5}}$) is $4.7 \times 10^{-3} \mu\text{g}^{2/3}$
508 W^{-1} . In both two plots, the black dashed lines are 1:1 lines. Correlation coefficients (R) and the relative errors (RE) are shown
509 in the legend.

510 4. Summary and Conclusions

511 In this study, long-term measurement of sulfuric acid from 2019 to 2021 was conducted in urban Beijing.
512 Daytime sulfuric acid concentration ranges from 2.0×10^6 to 7.4×10^6 molec cm^{-3} and shows a general declining trend,
513 with an average annual decrease of 14%, which is mainly due to SO_2 reduction. In addition, sulfuric acid
514 concentration shows a clear seasonal variation that tracks UVB, reaching the highest in May and September and
515 decreasing to the lowest from November to February of next year. In July and August, frequent precipitation lowers
516 UVB and SO_2 , resulting in lower sulfuric acid. Nighttime sulfuric acid concentration ranges from 1.6×10^5 to 6.3×10^5
517 molec cm^{-3} , about one order of magnitude lower than daytime. In warmer seasons, the sources of nighttime sulfuric
518 acid, such as benzene-related emissions and alkene ozonolysis, are stronger, and the losses are weaker, leading to
519 higher sulfuric acid level. The diurnal variations of photo-oxidation related parameters deviate slightly from sulfuric
520 acid. Sulfuric acid peaks earliest, followed by $\text{J}(\text{NO}_2)$, $\text{J}(\text{O}^1\text{D})$, UVB, global radiation, and OH radical. Meanwhile,
521 the peak width of sulfuric acid is the widest, followed by $\text{J}(\text{NO}_2)$, global radiation, OH radical, $\text{J}(\text{O}^1\text{D})$, and UVB.

522 The challenges in sulfuric acid measurement hinder its widespread observation. To obtain sulfuric acid proxies
523 applicable to most sites, we derive three sulfuric acid proxies directly from its steady-state budget analysis, named
524 as OH-CS based, UVB-CS based, and UVB- $\text{PM}_{2.5}$ based proxies. All three proxies perform well in estimating
525 sulfuric acid concentration during 10:00–14:00. We also evaluate the performance of nine sulfuric acid proxies
526 proposed in previous studies: seven based on formation and loss pathways (Petäjä et al., 2009; Dada et al., 2020)
527 and two derived from numerical regression (Mikkonen et al., 2011; Lu et al., 2019). Results show that $\text{Proxy}_{\text{Petäjä OH-C}}$
528 and $\text{Proxy}_{\text{Petäjä OH-F}}$ generally reproduce daytime sulfuric acid concentrations well, with estimated concentrations
529 closet to the measured one, correlation coefficients being 0.97 and 0.78, respectively, and relative errors being 74%
530 and 35%, respectively. However, the scaling factors therein are obtained by fitting the proxy equations. Thus, these
531 scaling factors are influenced by measurement reliability and have limited applicability at other sites. By contrast,
532 our proxies are derived directly from sulfuric acid budget analysis, and the parameters in the proxy equations are
533 transferable that can be used at a boreal forest site in Hyytiälä, Finland. Therefore, the three proxies developed in
534 this study have high potential for estimating daytime sulfuric acid concentrations at various sites.

535 It should be noted that the OH radical used in this study is not measured, but derived from a model simulation.
536 Under this circumstance, the OH-CS based proxy generally performs well, but has some deviations when OH radical
537 is in the range of $1.2\text{--}1.6 \times 10^7$ molec cm^{-3} and CS is lower than 0.015 s^{-1} . Although three steady-state-based proxies
538 generally perform well, they are not suitable under certain conditions. When OH radical, UVB and SO_2 are too low,
539 when CS and $\text{PM}_{2.5}$ are too high, or when RH exceeds 60%, estimated sulfuric acid concentration may deviate from
540 the actual concentration to a larger extent. Moreover, three proxies cannot fully reproduce sulfuric acid

541 concentration in early morning and at nightfall. This indicates that during these two periods, other sulfuric acid
542 sources, such as direct emission, alkenes ozonolysis and other formation pathways, are also important.

543 Here are some suggestions for the selection of three proxies. If one site has comprehensive measurement of OH
544 radical, particle size distribution and SO₂, the OH-CS based proxy illustrated by Eq. (16) is preferred, since it
545 estimates daytime concentration well and partly captures diurnal variation and nighttime sulfuric acid. Moreover,
546 the pre-factor in Eq. (16) is the actual OH + SO₂ reaction rate, making it suitable to all atmospheric sites. Then, if
547 OH radical is not directly measured, but UVB, SO₂, and particle size distribution are available, the UVB-CS based
548 proxy illustrated by Eq. (17) is preferred. Although it cannot perfectly trace the diurnal variation of sulfuric acid, it
549 estimates daytime concentration well. Moreover, because its pre-factor is transferable, it is convenient and
550 straightforward to use. Finally, if neither OH radical nor particle size distribution is measured, but UVB, SO₂, and
551 PM_{2.5} are available, the UVB-PM_{2.5} based proxy should be the right choice. These three parameters used are
552 commonly measured, giving this proxy broad applicability. Noted that $k_{UVB-PM_{2.5}}$ in Eq. (18) varies across sites.
553 For better accuracy, short-term synchronous measurement of particle size distribution and PM_{2.5} is suggested for
554 obtaining the pre-factor (k) in $CS = k \cdot PM_{2.5}^{2/3}$ and then correcting $k_{UVB-PM_{2.5}}$.

555 The acquisition of fundamental sulfuric acid concentration datasets is of great significance for elucidating the
556 global spatial distribution and long-term temporal trends of sulfuric acid. This may further promote researches on
557 the mechanisms of atmospheric nucleation, cluster growth, secondary aerosol formation, and pollution event
558 evolution at corresponding regions.

559

560 **Data and materials availability:** Datasets for this paper can be accessed at <https://zenodo.org/records/17216660>
561 (Guo et al., 2025).

562

563 **Author contributions:**

564 YG, CY and YL designed the study and wrote the paper. CL, CD, YZhang, YZhou, XC, WM, NS, ZL, CH, XF,
565 FZ, ZF, ZW, and YZ conducted the measurement and collected the data. HZ and YJ did the modelling. JJ, BZ and
566 MK are acknowledged for valuable suggestions. And co-authors have read and commented on the paper.

567

568 **Competing interests:** The authors declare that they have no conflict of interests.

569

570 **Acknowledgements and funds:** This study is funded by the National Natural Science Foundation of China (NSFC)
571 (grant No. 22327806), the Science and Technology Project of Hebei Education Department (grant No. QN2025049),
572 and the Doctoral Fund of Hebei Vocational University of Industry and Technology (No. bz202402).

573

- 575 Aalto, P., Hämeri, K., Becker, E., Weber, R., Salm, J., Mäkelä, J. M., Hoell, C., O’Dowd, C. D., Hansson, H.-C., Väkevä, M.,
576 Koponen, I. K., Buzorius, G., and Kulmala, M.: Physical characterization of aerosol particles during nucleation events, *Tellus*
577 *B: Chemical and Physical Meteorology*, 53, 344-358, 10.3402/tellusb.v53i4.17127, 2001.
- 578 Almeida, J., Schobesberger, S., Kuerten, A., Ortega, I. K., Kupiainen-Maatta, O., Praplan, A. P., Adamov, A., Amorim, A.,
579 Bianchi, F., Breitenlechner, M., David, A., Dommen, J., Donahue, N. M., Downard, A., Dunne, E., Duplissy, J., Ehrhart, S.,
580 Flagan, R. C., Franchin, A., Guida, R., Hakala, J., Hansel, A., Heinritzi, M., Henschel, H., Jokinen, T., Junninen, H., Kajos,
581 M., Kangasluoma, J., Keskinen, H., Kupc, A., Kurten, T., Kvashin, A. N., Laaksonen, A., Lehtipalo, K., Leiminger, M., Leppä,
582 J., Loukonen, V., Makhmutov, V., Mathot, S., McGrath, M. J., Nieminen, T., Olenius, T., Onnela, A., Petaja, T., Riccobono,
583 F., Riipinen, I., Rissanen, M., Rondo, L., Ruuskanen, T., Santos, F. D., Sarnela, N., Schallhart, S., Schnitzhofer, R., Seinfeld,
584 J. H., Simon, M., Sipila, M., Stozhkov, Y., Stratmann, F., Tome, A., Troestl, J., Tsagkogeorgas, G., Vaattovaara, P., Viisanen,
585 Y., Virtanen, A., Vrtala, A., Wagner, P. E., Weingartner, E., Wex, H., Williamson, C., Wimmer, D., Ye, P., Yli-Juuti, T.,
586 Carslaw, K. S., Kulmala, M., Curtius, J., Baltensperger, U., Worsnop, D. R., Vehkamäki, H., and Kirkby, J.: Molecular
587 understanding of sulphuric acid-amine particle nucleation in the atmosphere, *Nature*, 502, 359-363, 10.1038/nature12663, 2013.
- 588 Atkinson, R., Baulch, D. L., Cox, R. A., Crowley, J. N., Hampson, R. F., Hynes, R. G., Jenkin, M. E., Rossi, M. J., and Troe,
589 J.: Evaluated kinetic and photochemical data for atmospheric chemistry: Volume I - gas phase reactions of O_x, HO_x, NO_x and
590 SO_x species, *Atmospheric Chemistry and Physics*, 4, 1461-1738, 10.5194/acp-4-1461-2004, 2004.
- 591 Berresheim, H., Eisele, F. L., Tanner, D. J., McInnes, L. M., Ramsey-Bell, D. C., and Covert, D. S.: Atmospheric sulfur
592 chemistry and cloud condensation nuclei (CCN) concentrations over the northeastern Pacific Coast, *Journal of Geophysical*
593 *Research: Atmospheres*, 98, 12701-12711, <https://doi.org/10.1029/93JD00815>, 1993.
- 594 Berresheim, H., Elste, T., Plass-Dülmer, C., Eiseleb, F. L., and Tanner, D. J.: Chemical ionization mass spectrometer for long-
595 term measurements of atmospheric OH and H₂SO₄, *International Journal of Mass Spectrometry*, 202, 91-109,
596 [https://doi.org/10.1016/S1387-3806\(00\)00233-5](https://doi.org/10.1016/S1387-3806(00)00233-5), 2000.
- 597 Berresheim, H., Elste, T., Tremmel, H. G., Allen, A. G., Hansson, H. C., Rosman, K., Dal Maso, M., Mäkelä, J. M., Kulmala,
598 M., and O’Dowd, C. D.: Gas-aerosol relationships of H₂SO₄, MSA, and OH: Observations in the coastal marine boundary layer
599 at Mace Head, Ireland, *Journal of Geophysical Research: Atmospheres*, 107, PAR 5-1-PAR 5-12,
600 <https://doi.org/10.1029/2000JD000229>, 2002.
- 601 Birmili, W., Berresheim, H., Plass-Dulmer, C., Elste, T., Gilge, S., Wiedensohler, A., and Uhrner, U.: The Hohenpeissenberg
602 aerosol formation experiment (HAFEX): A long-term study including size-resolved aerosol, H₂SO₄, OH, and monoterpenes
603 measurements, *Atmospheric Chemistry and Physics*, 3, 361-376, 10.5194/acp-3-361-2003, 2003.
- 604 Boy, M., Karl, T., Turnipseed, A., Mauldin, R. L., Kosciuch, E., Greenberg, J., Rathbone, J., Smith, J., Held, A., Barsanti, K.,
605 Wehner, B., Bauer, S., Wiedensohler, A., Bonn, B., Kulmala, M., and Guenther, A.: New particle formation in the front range
606 of the Colorado rocky mountains, *Atmospheric Chemistry and Physics*, 8, 1577-1590, 10.5194/acp-8-1577-2008, 2008.
- 607 Chang, X., Zheng, H., Zhao, B., Yan, C., Jiang, Y., Hu, R., Song, S., Dong, Z., Li, S., Li, Z., Zhu, Y., Shi, H., Jiang, Z., Xing,
608 J., and Wang, S.: Drivers of High Concentrations of Secondary Organic Aerosols in Northern China during the COVID-19
609 Lockdowns, *Environmental Science & Technology*, 57, 5521-5531, 10.1021/acs.est.2c06914, 2023.
- 610 Chu, B., Kerminen, V. M., Bianchi, F., Yan, C., Petäjä, T., and Kulmala, M.: Atmospheric new particle formation in China,
611 *Atmospheric Chemistry and Physics*, 19, 115-138, 10.5194/acp-19-115-2019, 2019.
- 612 Dada, L., Paasonen, P., Nieminen, T., Buenrostro Mazon, S., Kontkanen, J., Peräkylä, O., Lehtipalo, K., Hussein, T., Petäjä,
613 T., Kerminen, V. M., Bäck, J., and Kulmala, M.: Long-term analysis of clear-sky new particle formation events and nonevents
614 in Hyytiälä, *Atmospheric Chemistry and Physics*, 17, 6227-6241, 10.5194/acp-17-6227-2017, 2017.
- 615 Dada, L., Ylivinkka, I., Baalbaki, R., Li, C., Guo, Y., Yan, C., Yao, L., Sarnela, N., Jokinen, T., Daellenbach, K. R., Yin, R.,
616 Deng, C., Chu, B., Nieminen, T., Kontkanen, J., Stolzenburg, D., Sipilä, M., Hussein, T., Paasonen, P., Bianchi, F., Salma, I.,
617 Weidinger, T., Pikridas, M., Sciare, J., Jiang, J., Liu, Y., Petäjä, T., Kerminen, V. M., and Kulmala, M.: Sources and sinks
618 driving sulphuric acid concentrations in contrasting environments: Implications on proxy calculations, *Atmospheric Chemistry*
619 *and Physics*, 20, 11747-11766, 10.5194/acp-20-11747-2020, 2020.
- 620 Dal Maso, M., Kulmala, M., Riipinen, I., and Wagner, R.: Formation and growth of fresh atmospheric aerosols: Eight years of
621 aerosol size distribution data from SMEAR II, Hyytiälä, Finland, *Boreal Environment Research*, 10, 323-336, 2005.

622 Deng, C., Fu, Y., Dada, L., Yan, C., Cai, R., Yang, D., Zhou, Y., Yin, R., Lu, Y., Li, X., Qiao, X., Fan, X., Nie, W., Kontkanen,
623 J., Kangasluoma, J., Chu, B., Ding, A., Kerminen, V.-M., Paasonen, P., Worsnop, D. R., Bianchi, F., Liu, Y., Zheng, J., Wang,
624 L., Kulmala, M., and Jiang, J.: Seasonal characteristics of new particle formation and growth in urban Beijing, *Environmental*
625 *Science & Technology*, 54, 8547-8557, 10.1021/acs.est.0c00808, 2020.

626 Erupe, M. E., Benson, D. R., Li, J., Young, L.-H., Verheggen, B., Al-Refai, M., Tahboub, O., Cunningham, V., Frimpong, F.,
627 Viggiano, A. A., and Lee, S.-H.: Correlation of aerosol nucleation rate with sulfuric acid and ammonia in Kent, Ohio: An
628 atmospheric observation, *Journal of Geophysical Research: Atmospheres*, 115, D23216, 10.1029/2010jd013942, 2010.

629 Fiedler, V., Dal Maso, M., Boy, M., Aufmhoff, H., Hoffmann, J., Schuck, T., Birmili, W., Hanke, M., Uecker, J., Arnold, F.,
630 and Kulmala, M.: The contribution of sulphuric acid to atmospheric particle formation and growth: A comparison between
631 boundary layers in Northern and Central Europe, *Atmospheric Chemistry and Physics*, 5, 1773-1785, 10.5194/acp-5-1773-
632 2005, 2005.

633 Finlayson-Pitts, B. J., and Pitts Jr., J. N.: *Chemistry of the Upper and Lower Atmosphere: Theory, Experiments, and*
634 *Applications*, Academic Press, San Diego, CA, USA, 298–299 pp., 2000.

635 Gordon, H., Kirkby, J., Baltensperger, U., Bianchi, F., Breitenlechner, M., Curtius, J., Dias, A., Dommen, J., Donahue, N. M.,
636 Dunne, E. M., Duplissy, J., Ehrhart, S., Flagan, R. C., Frege, C., Fuchs, C., Hansel, A., Hoyle, C. R., Kulmala, M., Kürten, A.,
637 Lehtipalo, K., Makhmutov, V., Molteni, U., Rissanen, M. P., Stozhkov, Y., Tröstl, J., Tsagkogeorgas, G., Wagner, R.,
638 Williamson, C., Wimmer, D., Winkler, P. M., Yan, C., and Carslaw, K. S.: Causes and importance of new particle formation
639 in the present-day and preindustrial atmospheres, *Journal of Geophysical Research: Atmospheres*, 122, 8739-8760,
640 <https://doi.org/10.1002/2017JD026844>, 2017.

641 Guo, Y., Yan, C., Li, C., Ma, W., Feng, Z., Zhou, Y., Lin, Z., Dada, L., Stolzenburg, D., Yin, R., Kontkanen, J., Daellenbach,
642 K. R., Kangasluoma, J., Yao, L., Chu, B., Wang, Y., Cai, R., Bianchi, F., Liu, Y., and Kulmala, M.: Formation of nighttime
643 sulfuric acid from the ozonolysis of alkenes in Beijing, *Atmospheric Chemistry and Physics*, 21, 5499-5511, 10.5194/acp-21-
644 5499-2021, 2021.

645 Jokinen, T., Sipilä, M., Junninen, H., Ehn, M., Lönn, G., Hakala, J., Petäjä, T., Mauldin Iii, R. L., Kulmala, M., and Worsnop,
646 D. R.: Atmospheric sulphuric acid and neutral cluster measurements using CI-API-TOF, *Atmospheric Chemistry and Physics*,
647 12, 4117-4125, 10.5194/acp-12-4117-2012, 2012.

648 Jokinen, T., Sipilä, M., Kontkanen, J., Vakkari, V., Tisler, P., Duplissy, E. M., Junninen, H., Kangasluoma, J., Manninen, H.
649 E., Petaja, T., Kulmala, M., Worsnop, D. R., Kirkby, J., Virkkula, A., and Kerminen, V. M.: Ion-induced sulfuric acid-ammonia
650 nucleation drives particle formation in coastal Antarctica, *Science Advances*, 4, eaat9744, 10.1126/sciadv.aat9744, 2018.

651 Kirkby, J., Curtius, J., Almeida, J., Dunne, E., Duplissy, J., Ehrhart, S., Franchin, A., Gagne, S., Ickes, L., Kuerten, A., Kupc,
652 A., Metzger, A., Riccobono, F., Rondo, L., Schobesberger, S., Tsagkogeorgas, G., Wimmer, D., Amorim, A., Bianchi, F.,
653 Breitenlechner, M., David, A., Dommen, J., Downard, A., Ehn, M., Flagan, R. C., Haider, S., Hansel, A., Hauser, D., Jud, W.,
654 Junninen, H., Kreissl, F., Kvashin, A., Laaksonen, A., Lehtipalo, K., Lima, J., Lovejoy, E. R., Makhmutov, V., Mathot, S.,
655 Mikkilä, J., Minginette, P., Mogo, S., Nieminen, T., Onnela, A., Pereira, P., Petaja, T., Schnitzhofer, R., Seinfeld, J. H., Sipilä,
656 M., Stozhkov, Y., Stratmann, F., Tome, A., Vanhanen, J., Viisanen, Y., Vrtala, A., Wagner, P. E., Walther, H., Weingartner,
657 E., Wex, H., Winkler, P. M., Carslaw, K. S., Worsnop, D. R., Baltensperger, U., and Kulmala, M.: Role of sulphuric acid,
658 ammonia and galactic cosmic rays in atmospheric aerosol nucleation, *Nature*, 476, 429-433, 10.1038/nature10343, 2011.

659 Kulmala, M., Lehtinen, K. E. J., and Laaksonen, A.: Cluster activation theory as an explanation of the linear dependence
660 between formation rate of 3nm particles and sulphuric acid concentration, *Atmospheric Chemistry and Physics*, 6, 787-793,
661 10.5194/acp-6-787-2006, 2006.

662 Kulmala, M., Riipinen, I., Sipilä, M., Manninen, H. E., Petäjä, T., Junninen, H., Maso, M. D., Mordas, G., Mirme, A., Vana,
663 M., Hirsikko, A., Laakso, L., Harrison, R. M., Hanson, I., Leung, C., Lehtinen, K. E. J., and Kerminen, V.-M.: Toward Direct
664 Measurement of Atmospheric Nucleation, *Science*, 318, 89-92, 10.1126/science.1144124, 2007.

665 Kulmala, M., Petäjä, T., Nieminen, T., Sipilä, M., Manninen, H. E., Lehtipalo, K., Dal Maso, M., Aalto, P. P., Junninen, H.,
666 Paasonen, P., Riipinen, I., Lehtinen, K. E. J., Laaksonen, A., and Kerminen, V.-M.: Measurement of the nucleation of
667 atmospheric aerosol particles, *Nature Protocols*, 7, 1651-1667, 10.1038/nprot.2012.091, 2012.

668 Kulmala, M., Kontkanen, J., Junninen, H., Lehtipalo, K., Manninen, H. E., Nieminen, T., Petäjä, T., Sipilä, M., Schobesberger,
669 S., Rantala, P., Franchin, A., Jokinen, T., Järvinen, E., Äijälä, M., Kangasluoma, J., Hakala, J., Aalto, P. P., Paasonen, P.,
670 Mikkilä, J., Vanhanen, J., Aalto, J., Hakola, H., Makkonen, U., Ruuskanen, T., Mauldin, R. L., Duplissy, J., Vehkamäki, H.,

671 Bäck, J., Kortelainen, A., Riipinen, I., Kurtén, T., Johnston, M. V., Smith, J. N., Ehn, M., Mentel, T. F., Lehtinen, K. E. J.,
672 Laaksonen, A., Kerminen, V.-M., and Worsnop, D. R.: Direct observations of atmospheric aerosol nucleation, *Science*, 339,
673 943-946, 10.1126/science.1227385, 2013.

674 Kürten, A., Rondo, L., Ehrhart, S., and Curtius, J.: Calibration of a Chemical Ionization Mass Spectrometer for the measurement
675 of gaseous sulfuric acid, *The Journal of Physical Chemistry A*, 116, 6375-6386, 10.1021/jp212123n, 2012.

676 Kürten, A., Jokinen, T., Simon, M., Sipila, M., Sarnela, N., Junninen, H., Adamov, A., Almeida, J., Amorim, A., Bianchi, F.,
677 Breitenlechner, M., Dommen, J., Donahue, N. M., Duplissy, J., Ehrhart, S., Flagan, R. C., Franchin, A., Hakala, J., Hansel, A.,
678 Heinritzi, M., Hutterli, M., Kangasluoma, J., Kirkby, J., Laaksonen, A., Lehtipalo, K., Leiminger, M., Makhmutov, V., Mathot,
679 S., Onnela, A., Petaja, T., Praplan, A. P., Riccobono, F., Rissanen, M. P., Rondo, L., Schobesberger, S., Seinfeld, J. H., Steiner,
680 G., Tome, A., Troestl, J., Winkler, P. M., Williamson, C., Wimmer, D., Ye, P., Baltensperger, U., Carslaw, K. S., Kulmala, M.,
681 Worsnop, D. R., and Curtius, J.: Neutral molecular cluster formation of sulfuric acid-dimethylamine observed in real time
682 under atmospheric conditions, *Proceedings of the National Academy of Sciences*, 111, 15019-15024,
683 10.1073/pnas.1404853111, 2014.

684 Kürten, A., Bergen, A., Heinritzi, M., Leiminger, M., Lorenz, V., Piel, F., Simon, M., Sitals, R., Wagner, A. C., and Curtius,
685 J.: Observation of new particle formation and measurement of sulfuric acid, ammonia, amines and highly oxidized organic
686 molecules at a rural site in central Germany, *Atmospheric Chemistry and Physics*, 16, 12793-12813, 10.5194/acp-16-12793-
687 2016, 2016.

688 Lee, S. H., Gordon, H., Yu, H., Lehtipalo, K., Haley, R., Li, Y. X., and Zhang, R. Y.: New particle formation in the atmosphere:
689 from molecular clusters to global climate, *Journal of Geophysical Research: Atmospheres*, 124, 7098-7146,
690 10.1029/2018jd029356, 2019.

691 Lehtipalo, K., Yan, C., Dada, L., Bianchi, F., Xiao, M., Wagner, R., Stolzenburg, D., Ahonen, L., Amorim, A., Baccarini, A.,
692 Bauer, P., Baumgartner, B., Bergen, A., Bernhammer, A.-K., Breitenlechner, M., Brilke, S., Buchholz, A., Mazon, S., Chen,
693 D., and Worsnop, D.: Multicomponent new particle formation from sulfuric acid, ammonia, and biogenic vapors, *Science*
694 *Advances*, 4, eaau5363, 10.1126/sciadv.aau5363, 2018.

695 Lelieveld, J., Evans, J. S., Fnais, M., Giannadaki, D., and Pozzer, A.: The contribution of outdoor air pollution sources to
696 premature mortality on a global scale, *Nature*, 525, 367-371, 10.1038/nature15371, 2015.

697 Liu, J., Jiang, J., Zhang, Q., Deng, J., and Hao, J.: A spectrometer for measuring particle size distributions in the range of 3 nm
698 to 10 μm , *Frontiers of Environmental Science & Engineering*, 10, 63-72, 10.1007/s11783-014-0754-x, 2016.

699 Liu, Y., Yan, C., Feng, Z., Zheng, F., Fan, X., Zhang, Y., Li, C., Zhou, Y., Lin, Z., Guo, Y., Zhang, Y., Ma, L., Zhou, W., Liu,
700 Z., Dada, L., Dällenbach, K., Kontkanen, J., Cai, R., Chan, T., Chu, B., Du, W., Yao, L., Wang, Y., Cai, J., Kangasluoma, J.,
701 Kokkonen, T., Kujansuu, J., Rusanen, A., Deng, C., Fu, Y., Yin, R., Li, X., Lu, Y., Liu, Y., Lian, C., Yang, D., Wang, W., Ge,
702 M., Wang, Y., Worsnop, D. R., Junninen, H., He, H., Kerminen, V.-M., Zheng, J., Wang, L., Jiang, J., Petäjä, T., Bianchi, F.,
703 and Kulmala, M.: Continuous and comprehensive atmospheric observations in Beijing: A station to understand the complex
704 urban atmospheric environment, *Big Earth Data*, 4, 295-321, 10.1080/20964471.2020.1798707, 2020.

705 Lu, K. D., Rohrer, F., Holland, F., Fuchs, H., Bohn, B., Brauers, T., Chang, C. C., Häsel, R., Hu, M., Kita, K., Kondo, Y., Li,
706 X., Lou, S. R., Nehr, S., Shao, M., Zeng, L. M., Wahner, A., Zhang, Y. H., and Hofzumahaus, A.: Observation and modelling
707 of OH and HO₂ concentrations in the Pearl River Delta 2006: A missing OH source in a VOC rich atmosphere, *Atmospheric*
708 *Chemistry and Physics*, 12, 1541-1569, 10.5194/acp-12-1541-2012, 2012.

709 Lu, Y., Yan, C., Fu, Y., Chen, Y., Liu, Y., Yang, G., Wang, Y., Bianchi, F., Chu, B., Zhou, Y., Yin, R., Baalbaki, R., Garmash,
710 O., Deng, C., Wang, W., Liu, Y., Petaja, T., Kerminen, V.-M., Jiang, J., Kulmala, M., and Wang, L.: A proxy for atmospheric
711 daytime gaseous sulfuric acid concentration in urban Beijing, *Atmospheric Chemistry and Physics*, 19, 1971-1983,
712 10.5194/acp-19-1971-2019, 2019.

713 Ma, L., Zhu, Y., Zheng, M., Sun, Y., Huang, L., Liu, X., Gao, Y., Shen, Y., Gao, H., and Yao, X.: Investigating three patterns
714 of new particles growing to the size of cloud condensation nuclei in Beijing's urban atmosphere, *Atmos. Chem. Phys.*, 21, 183-
715 200, 10.5194/acp-21-183-2021, 2021.

716 Ma, X., Tan, Z., Lu, K., Yang, X., Liu, Y., Li, S., Li, X., Chen, S., Novelli, A., Cho, C., Zeng, L., Wahner, A., and Zhang, Y.:
717 Winter photochemistry in Beijing: Observation and model simulation of OH and HO₂ radicals at an urban site, *Science of The*
718 *Total Environment*, 685, 85-95, <https://doi.org/10.1016/j.scitotenv.2019.05.329>, 2019.

719 Ma, X., Tan, Z., Lu, K., Yang, X., Chen, X., Wang, H., Chen, S., Fang, X., Li, S., Li, X., Liu, J., Liu, Y., Lou, S., Qiu, W.,
720 Wang, H., Zeng, L., and Zhang, Y.: OH and HO₂ radical chemistry at a suburban site during the EXPLORE-YRD campaign
721 in 2018, *Atmospheric Chemistry and Physics*, 22, 7005-7028, 10.5194/acp-22-7005-2022, 2022.

722 Manninen, H. E., Nieminen, T., Riipinen, I., Yli-Juuti, T., Gagné, S., Asmi, E., Aalto, P. P., Petäjä, T., Kerminen, V. M., and
723 Kulmala, M.: Charged and total particle formation and growth rates during EUCAARI 2007 campaign in Hyytiälä,
724 *Atmospheric Chemistry and Physics*, 9, 4077-4089, 10.5194/acp-9-4077-2009, 2009.

725 Mauldin, R. L., Eisele, F. L., Tanner, D. J., Kosciuch, E., Shetter, R., Lefer, B., Hall, S. R., Nowak, J. B., Buhr, M., Chen, G.,
726 Wang, P., and Davis, D.: Measurements of OH, H₂SO₄, and MSA at the South Pole during ISCAT, *Geophysical Research*
727 *Letters*, 28, 3629-3632, 10.1029/2000gl012711, 2001.

728 Mauldin, R. L., Kosciuch, E., Henry, B., Eisele, F. L., Shetter, R., Lefer, B., Chen, G., Davis, D., Huey, G., and Tanner, D.:
729 Measurements of OH, HO₂+RO₂, H₂SO₄, and MSA at the South Pole during ISCAT 2000, *Atmospheric Environment*, 38,
730 5423-5437, <https://doi.org/10.1016/j.atmosenv.2004.06.031>, 2004.

731 McMurry, P. H., Fink, M., Sakurai, H., Stolzenburg, M. R., Mauldin, R. L., Smith, J., Eisele, F., Moore, K., Sjostedt, S., Tanner,
732 D., Huey, L. G., Nowak, J. B., Edgerton, E., and Voisin, D.: A criterion for new particle formation in the sulfur-rich Atlanta
733 atmosphere, *Journal of Geophysical Research: Atmospheres*, 110, D22S02, 10.1029/2005jd005901, 2005.

734 Merikanto, J., Spracklen, D. V., Mann, G. W., Pickering, S. J., and Carslaw, K. S.: Impact of nucleation on global CCN,
735 *Atmospheric Chemistry and Physics*, 9, 8601-8616, 10.5194/acp-9-8601-2009, 2009.

736 Mikkonen, S., Romakkaniemi, S., Smith, J. N., Korhonen, H., Petäjä, T., Plass-Duelmer, C., Boy, M., McMurry, P. H., Lehtinen,
737 K. E. J., Joutsensaari, J., Hamed, A., Mauldin III, R. L., Birmili, W., Spindler, G., Arnold, F., Kulmala, M., and Laaksonen, A.:
738 A statistical proxy for sulphuric acid concentration, *Atmospheric Chemistry and Physics*, 11, 11319-11334, 10.5194/acp-11-
739 11319-2011, 2011.

740 Myllys, N., Chee, S., Olenius, T., Lawler, M., and Smith, J.: Molecular-level understanding of synergistic effects in sulfuric
741 acid-amine-ammonia mixed clusters, *The Journal of Physical Chemistry A*, 123, 2420-2425, 10.1021/acs.jpca.9b00909, 2019.

742 Nieminen, T., Manninen, H. E., Sihto, S. L., Yli-Juuti, T., Mauldin, I. R. L., Petäjä, T., Riipinen, I., Kerminen, V. M., and
743 Kulmala, M.: Connection of sulfuric acid to atmospheric nucleation in boreal forest, *Environmental Science & Technology*,
744 43, 4715-4721, 10.1021/es803152j, 2009.

745 Nieminen, T., Kerminen, V. M., Petäjä, T., Aalto, P. P., Arshinov, M., Asmi, E., Baltensperger, U., Beddows, D. C. S., Beukes,
746 J. P., Collins, D., Ding, A., Harrison, R. M., Henzing, B., Hooda, R., Hu, M., Hörrak, U., Kivekäs, N., Komsaare, K., Krejci,
747 R., Kristensson, A., Laakso, L., Laaksonen, A., Leitch, W. R., Lihavainen, H., Mihalopoulos, N., Németh, Z., Nie, W.,
748 O'Dowd, C., Salma, I., Sellegri, K., Svenningsson, B., Swietlicki, E., Tunved, P., Ulevicius, V., Vakkari, V., Vana, M.,
749 Wiedensohler, A., Wu, Z., Virtanen, A., and Kulmala, M.: Global analysis of continental boundary layer new particle formation
750 based on long-term measurements, *Atmospheric Chemistry and Physics*, 18, 14737-14756, 10.5194/acp-18-14737-2018, 2018.

751 O'Dowd, C. D., Aalto, P., Hmeri, K., Kulmala, M., and Hoffmann, T.: Atmospheric particles from organic vapours, *Nature*,
752 416, 497-498, 10.1038/416497a, 2002.

753 Paasonen, P., Sihto, S.-L., Nieminen, T., Vuollekoski, H., Riipinen, I., Plass-Dulmer, C., Berresheim, H., Birmili, W., and
754 Kulmala, M.: Connection between new particle formation and sulphuric acid at Hohenpeissenberg (Germany) including the
755 influence of organic compounds, *Boreal Environment Research*, 14, 616-629, 2009.

756 Petäjä, T., Mauldin, I. R. L., Kosciuch, E., McGrath, J., Nieminen, T., Paasonen, P., Boy, M., Adamov, A., Kotiaho, T., and
757 Kulmala, M.: Sulfuric acid and OH concentrations in a boreal forest site, *Atmospheric Chemistry and Physics*, 9, 7435-7448,
758 10.5194/acp-9-7435-2009, 2009.

759 Qi, X. M., Ding, A. J., Nie, W., Petäjä, T., Kerminen, V. M., Herrmann, E., Xie, Y. N., Zheng, L. F., Manninen, H., Aalto, P.,
760 Sun, J. N., Xu, Z. N., Chi, X. G., Huang, X., Boy, M., Virkkula, A., Yang, X. Q., Fu, C. B., and Kulmala, M.: Aerosol size
761 distribution and new particle formation in the western Yangtze River Delta of China: 2 years of measurements at the SORPES
762 station, *Atmospheric Chemistry and Physics*, 15, 12445-12464, 10.5194/acp-15-12445-2015, 2015.

763 Riccobono, F., Schobesberger, S., Scott, C., Dommen, J., Ortega, I., Rondo, L., Almeida, J., Amorim, A., Bianchi, F.,
764 Breitenlechner, M., David, A., Downard, A., Dunne, E., Duplissy, J., Ehrhart, S., Flagan, R., Franchin, A., Hansel, A., Junninen,
765 H., and Baltensperger, U.: Oxidation products of biogenic emissions contribute to nucleation of atmospheric particles, *Science*,
766 344, 717-721, 10.1126/science.1243527, 2014.

767 Riipinen, I., Sihto, S. L., Kulmala, M., Arnold, F., Dal Maso, M., Birmili, W., Saarnio, K., Teinila, K., Kerminen, V. M.,
768 Laaksonen, A., and Lehtinen, K. E. J.: Connections between atmospheric sulphuric acid and new particle formation during
769 QUEST III-IV campaigns in Heidelberg and Hyytiälä, *Atmospheric Chemistry and Physics*, 7, 1899-1914, 10.5194/acp-7-
770 1899-2007, 2007.

771 Rohrer, F., and Berresheim, H.: Strong correlation between levels of tropospheric hydroxyl radicals and solar ultraviolet
772 radiation, *Nature*, 442, 184-187, 10.1038/nature04924, 2006.

773 Sarnela, N., Jokinen, T., Nieminen, T., Lehtipalo, K., Junninen, H., Kangasluoma, J., Hakala, J., Taipale, R., Schobesberger,
774 S., Sipila, M., Larnimaa, K., Westerholm, H., Heijari, J., Kerminen, V.-M., Petaja, T., and Kulmala, M.: Sulphuric acid and
775 aerosol particle production in the vicinity of an oil refinery, *Atmospheric Environment*, 119, 156-166,
776 10.1016/j.atmosenv.2015.08.033, 2015.

777 Sarwar, G., Appel, K. W., Carlton, A. G., Mathur, R., Schere, K., Zhang, R., and Majeed, M. A.: Impact of a new condensed
778 toluene mechanism on air quality model predictions in the US, *Geosci. Model Dev.*, 4, 183-193, 10.5194/gmd-4-183-2011,
779 2011.

780 Stocker, T.: *Climate change 2013: the physical science basis: Working Group I contribution to the Fifth assessment report of*
781 *the Intergovernmental Panel on Climate Change*, 2014.

782 Tan, Z., Fuchs, H., Lu, K., Hofzumahaus, A., Bohn, B., Broch, S., Dong, H., Gomm, S., Häsel, R., He, L., Holland, F., Li,
783 X., Liu, Y., Lu, S., Rohrer, F., Shao, M., Wang, B., Wang, M., Wu, Y., Zeng, L., Zhang, Y., Wahner, A., and Zhang, Y.:
784 Radical chemistry at a rural site (Wangdu) in the North China Plain: Observation and model calculations of OH, HO₂ and RO₂
785 radicals, *Atmospheric Chemistry and Physics*, 17, 663-690, 10.5194/acp-17-663-2017, 2017.

786 Tan, Z., Rohrer, F., Lu, K., Ma, X., Bohn, B., Broch, S., Dong, H., Fuchs, H., Gkatzelis, G. I., Hofzumahaus, A., Holland, F.,
787 Li, X., Liu, Y., Liu, Y., Novelli, A., Shao, M., Wang, H., Wu, Y., Zeng, L., Hu, M., Kiendler-Scharr, A., Wahner, A., and
788 Zhang, Y.: Wintertime photochemistry in Beijing: Observations of RO_x radical concentrations in the North China Plain during
789 the BEST-ONE campaign, *Atmospheric Chemistry and Physics*, 18, 12391-12411, 10.5194/acp-18-12391-2018, 2018.

790 Wang, Z. B., Hu, M., Yue, D. L., Zheng, J., Zhang, R. Y., Wiedensohler, A., Wu, Z. J., Nieminen, T., and Boy, M.: Evaluation
791 on the role of sulfuric acid in the mechanisms of new particle formation for Beijing case, *Atmospheric Chemistry and Physics*,
792 11, 12663-12671, 10.5194/acp-11-12663-2011, 2011.

793 Weber, R. J., McMurry, P., H. J. J. o. t. A. S.: Measurement of expected nucleation precursor species and 3-500-nm
794 diameter particles at Mauna Loa, 1995.

795 Weber, R. J., Marti, J. J., McMurry, P. H., Eisele, F. L., Tanner, D. J., and Jefferson, A.: Measured atmospheric new particle
796 formation rates: Implications for nucleation mechanisms, *Chemical Engineering Communications*, 151, 53-64, 1996.

797 Weber, R. J., Marti, J. J., McMurry, P. H., Eisele, F. L., Tanner, D. J., and Jefferson, A.: Measurements of new particle
798 formation and ultrafine particle growth rates at a clean continental site, *Journal of Geophysical Research: Atmospheres*, 102,
799 4375-4385, 10.1029/96jd03656, 1997.

800 Weber, R. J., McMurry, P. H., Mauldin, L., Tanner, D. J., Eisele, F. L., Brechtel, F. J., Kreidenweis, S. M., Kok, G. L.,
801 Schillawski, R. D., and Baumgardner, D.: A study of new particle formation and growth involving biogenic and trace gas
802 species measured during ACE 1, *Journal of Geophysical Research: Atmospheres*, 103, 16385-16396, 10.1029/97jd02465, 1998.

803 Wine, P. H., Thompson, R. J., Ravishankara, A. R., Semmes, D. H., Gump, C. A., Torabi, A., and Nicovich, J. M.: *Journal of*
804 *Physical Chemistry*, 88, 2104-2109, 1984.

805 Yan, C., Yin, R., Lu, Y., Dada, L., Yang, D., Fu, Y., Kontkanen, J., Deng, C., Garmash, O., Ruan, J., Baalbaki, R., Schervish,
806 M., Cai, R., Bloss, M., Chan, T., Chen, T., Chen, Q., Chen, X., Chen, Y., Chu, B., Dällenbach, K., Foreback, B., He, X.,
807 Heikkinen, L., Jokinen, T., Junninen, H., Kangasluoma, J., Kokkonen, T., Kurppa, M., Lehtipalo, K., Li, H., Li, H., Li, X., Liu,
808 Y., Ma, Q., Paasonen, P., Rantala, P., Pileci, R. E., Rusanen, A., Sarnela, N., Simonen, P., Wang, S., Wang, W., Wang, Y.,
809 Xue, M., Yang, G., Yao, L., Zhou, Y., Kujansuu, J., Petäjä, T., Nie, W., Ma, Y., Ge, M., He, H., Donahue, N. M., Worsnop, D.
810 R., Veli-Matti, K., Wang, L., Liu, Y., Zheng, J., Kulmala, M., Jiang, J., and Bianchi, F.: The synergistic role of sulfuric acid,
811 bases, and oxidized organics governing new-particle formation in Beijing, *Geophysical Research Letters*, 48, e2020GL091944,
812 <https://doi.org/10.1029/2020GL091944>, 2021.

813 Yan, C., Shen, Y., Stolzenburg, D., Dada, L., Qi, X., Hakala, S., Sundström, A. M., Guo, Y., Lipponen, A., Kokkonen, T.,
814 Kontkanen, J., Cai, R., Cai, J., Chan, T., Chen, L., Chu, B., Deng, C., Du, W., Fan, X., He, X. C., Kangasluoma, J., Kujansuu,
815 J., Kurppa, M., Li, C., Li, Y., Lin, Z., Liu, Y., Liu, Y., Lu, Y., Nie, W., Pulliainen, J., Qiao, X., Wang, Y., Wen, Y., Wu, Y.,

816 Yang, G., Yao, L., Yin, R., Zhang, G., Zhang, S., Zheng, F., Zhou, Y., Arola, A., Tamminen, J., Paasonen, P., Sun, Y., Wang,
817 L., Donahue, N. M., Liu, Y., Bianchi, F., Daellenbach, K. R., Worsnop, D. R., Kerminen, V. M., Petäjä, T., Ding, A., Jiang, J.,
818 and Kulmala, M.: The effect of COVID-19 restrictions on atmospheric new particle formation in Beijing, *Atmos. Chem. Phys.*
819 *Discuss.*, 2022, 1-24, [10.5194/acp-2021-1079](https://doi.org/10.5194/acp-2021-1079), 2022.

820 Yang, C., Dong, H., Chen, Y., Wang, Y., Fan, X., Tham, Y. J., Chen, G., Xu, L., Lin, Z., Li, M., Hong, Y., and Chen, J.:
821 Machine Learning Reveals the Parameters Affecting the Gaseous Sulfuric Acid Distribution in a Coastal City: Model
822 Construction and Interpretation, *Environmental Science & Technology Letters*, 10, 1045-1051, [10.1021/acs.estlett.3c00170](https://doi.org/10.1021/acs.estlett.3c00170),
823 2023.

824 Yang, L., Nie, W., Liu, Y., Xu, Z., Xiao, M., Qi, X., Li, Y., Wang, R., Zou, J., Paasonen, P., Yan, C., Xu, Z., Wang, J., Zhou,
825 C., Yuan, J., Sun, J., Chi, X., Kerminen, V.-M., Kulmala, M., and Ding, A.: Toward building a physical proxy for gas-phase
826 sulfuric acid concentration based on its budget analysis in polluted Yangtze River Delta, East China, *Environmental Science*
827 *& Technology*, 55, 6665-6676, [10.1021/acs.est.1c00738](https://doi.org/10.1021/acs.est.1c00738), 2021a.

828 Yang, X., Lu, K., Ma, X., Liu, Y., Wang, H., Hu, R., Li, X., Lou, S., Chen, S., Dong, H., Wang, F., Wang, Y., Zhang, G., Li,
829 S., Yang, S., Yang, Y., Kuang, C., Tan, Z., Chen, X., Qiu, P., Zeng, L., Xie, P., and Zhang, Y.: Observations and modeling of
830 OH and HO₂ radicals in Chengdu, China in summer 2019, *Science of The Total Environment*, 772, 144829,
831 <https://doi.org/10.1016/j.scitotenv.2020.144829>, 2021b.

832 Yao, L., Garmash, O., Bianchi, F., Zheng, J., Yan, C., Kontkanen, J., Junninen, H., Mazon, S. B., Ehn, M., Paasonen, P., Sipila,
833 M., Wang, M. Y., Wang, X. K., Xiao, S., Chen, H. F., Lu, Y. Q., Zhang, B. W., Wang, D. F., Fu, Q. Y., Geng, F. H., Li, L.,
834 Wang, H. L., Qiao, L. P., Yang, X., Chen, J. M., Kerminen, V. M., Petaja, T., Worsnop, D. R., Kulmala, M., and Wang, L.:
835 Atmospheric new particle formation from sulfuric acid and amines in a Chinese megacity, *Science*, 361, 278-281,
836 [10.1126/science.aao4839](https://doi.org/10.1126/science.aao4839), 2018.

837 Yao, L., Fan, X., Yan, C., Kurtén, T., Daellenbach, K. R., Li, C., Wang, Y., Guo, Y., Dada, L., Rissanen, M. P., Cai, J., Tham,
838 Y. J., Zha, Q., Zhang, S., Du, W., Yu, M., Zheng, F., Zhou, Y., Kontkanen, J., Chan, T., Shen, J., Kujansuu, J. T., Kangasluoma,
839 J., Jiang, J., Wang, L., Worsnop, D. R., Petäjä, T., Kerminen, V.-M., Liu, Y., Chu, B., He, H., Kulmala, M., and Bianchi, F.:
840 Unprecedented ambient sulfur trioxide (SO₃) detection: Possible formation mechanism and atmospheric implications,
841 *Environmental Science & Technology Letters*, 7, 809-818, [10.1021/acs.estlett.0c00615](https://doi.org/10.1021/acs.estlett.0c00615), 2020.

842 Yu, H., McGraw, R., and Lee, S.-H.: Effects of amines on formation of sub-3 nm particles and their subsequent growth,
843 *Geophysical Research Letters*, 39, [10.1029/2011gl050099](https://doi.org/10.1029/2011gl050099), 2012.

844 Zhao, B., Wang, S., Donahue, N. M., Jathar, S. H., Huang, X., Wu, W., Hao, J., and Robinson, A. L.: Quantifying the effect of
845 organic aerosol aging and intermediate-volatility emissions on regional-scale aerosol pollution in China, *Scientific Reports*, 6,
846 28815, [10.1038/srep28815](https://doi.org/10.1038/srep28815), 2016.

847 Zhao, B., Zheng, H., Wang, S., Smith, K. R., Lu, X., Aunan, K., Gu, Y., Wang, Y., Ding, D., Xing, J., Fu, X., Yang, X., Liou,
848 K.-N., and Hao, J.: Change in household fuels dominates the decrease in PM_{2.5} exposure and premature mortality in China in
849 2005–2015, *Proceedings of the National Academy of Sciences*, 115, 12401-12406, [10.1073/pnas.1812955115](https://doi.org/10.1073/pnas.1812955115), 2018.

850 Zheng, H., Cai, S., Wang, S., Zhao, B., Chang, X., and Hao, J.: Development of a unit-based industrial emission inventory in
851 the Beijing–Tianjin–Hebei region and resulting improvement in air quality modeling, *Atmos. Chem. Phys.*, 19, 3447-3462,
852 [10.5194/acp-19-3447-2019](https://doi.org/10.5194/acp-19-3447-2019), 2019a.

853 Zheng, H., Zhao, B., Wang, S., Wang, T., Ding, D., Chang, X., Liu, K., Xing, J., Dong, Z., Aunan, K., Liu, T., Wu, X., Zhang,
854 S., and Wu, Y.: Transition in source contributions of PM_{2.5} exposure and associated premature mortality in China during 2005–
855 2015, *Environment International*, 132, 105111, <https://doi.org/10.1016/j.envint.2019.105111>, 2019b.

856 Zheng, H., Song, S., Sarwar, G., Gen, M., Wang, S., Ding, D., Chang, X., Zhang, S., Xing, J., Sun, Y., Ji, D., Chan, C. K., Gao,
857 J., and McElroy, M. B.: Contribution of Particulate Nitrate Photolysis to Heterogeneous Sulfate Formation for Winter Haze in
858 China, *Environmental Science & Technology Letters*, 7, 632-638, [10.1021/acs.estlett.0c00368](https://doi.org/10.1021/acs.estlett.0c00368), 2020.

859 Zheng, H., Chang, X., Wang, S., Li, S., Zhao, B., Dong, Z., Ding, D., Jiang, Y., Huang, G., Huang, C., An, J., Zhou, M., Qiao,
860 L., and Xing, J.: Sources of Organic Aerosol in China from 2005 to 2019: A Modeling Analysis, *Environmental Science &*
861 *Technology*, 57, 5957-5966, [10.1021/acs.est.2c08315](https://doi.org/10.1021/acs.est.2c08315), 2023.

862 Zheng, H., Li, S., Jiang, Y., Dong, Z., Yin, D., Zhao, B., Wu, Q., Liu, K., Zhang, S., Wu, Y., Wen, Y., Xing, J., Henneman, L.
863 R. F., Kinney, P. L., Wang, S., and Hao, J.: Unpacking the factors contributing to changes in PM_{2.5}-associated mortality in
864 China from 2013 to 2019, *Environment International*, 184, 108470, <https://doi.org/10.1016/j.envint.2024.108470>, 2024.

